Research article **Rev. Cong. Sci. Technol., Vol. 05, No. 04, pp. 1749-1770 (2026)**

OPEN ACCESS

Revue Congolaise des Sciences & Technologies

ISSN : 2959-202X (Online); 2960-2629 (Print)

https://www.csnrdc.net/

REVUE CONGOLAISE DES SCIENCES ET TECHNOLOGIES

Spatio-Temporal Dynamics of the Mayombe Forest (2000–2025) in Mvouti (Kouilou, Republic of the Congo): A Remote Sensing and CA-Markov Modeling Analysis Through 2050

[Dynamique spatio-temporelle de la forêt du Mayombe (2000–2025) à Mvouti (Kouilou, République du Congo) : Une analyse par télédétection et modélisation CA-Markov à l'horizon 2050]

Cédrick Belmich Nkoua Ondon[1*], Jessy Houston Tchoffo Tsoala[1], Joseph Otshinga Abedi[1], Michel Omeno Opelele[1], Papy-Claude Boliale Bolaluembe[1], Raphael Muamba Tshimanga[1,3], Aimé Patrick Lola Missamba[2], Roger Vumilia Kizungu[1], Bonaventure Nyami LeLe[1] & Eric Landui Lutete[1]

[1]University of Kinshasa, Faculty of Agronomic Sciences and Environment, Department of Natural Resource Management, P.O. Box 117 Kinshasa XI, Mont Amba District, Democratic Republic of the Congo

[2]Research Center on Sustainability and Industrial Plantations (CRDPI), Marien Ngouabi University, Faculty of Science and Technology, Republic of the Congo

[3]Congo Basin Water Resources Research and Capacity-Building Center (CRREBaC), Democratic Republic of the Congo

Abstract

The Mvouti district, located in the Kouilou department (Republic of the Congo), harbors a critical portion of the Mayombe forest massif, which encompasses the Dimonika Biosphere Reserve (136,000 ha, UNESCO-MAB 1988). This reserve was selected as it represents a biodiversity hotspot under severe anthropogenic pressures from artisanal gold mining and logging. Using six Landsat image composites (2000–2025, 30 m spatial resolution) classified into a five-class land-use/land-cover nomenclature via the Random Forest algorithm on Google Earth Engine, this article quantifies the spatio-temporal dynamics of forest cover, analyzes the fragmentation of the massif, and simulates three prospective trajectories through 2050 using CA-Markov modeling. With an overall classification accuracy of 90.6% (κ mean = 0.883), dense forest lost 32,106 ha (9.1% of the initial cover) between 2000 and 2025. The mean deforestation rate is estimated at 0.37%/year, three to four times higher than the Congolese national average. Disaggregation by land tenure status reveals contrasting dynamics: areas outside logging concessions peaked at 2.27%/year between 2015 and 2020, while managed concessions (FMUs) within the reserve buffer zone maintained significantly lower rates. Fragmentation intensified sharply (patch count rose from 442 to 6,189; MESH: −21.5%). Under the integrated governance scenario (SC3, consistent with Law No. 33-2020 and the Nationally Determined Contribution [NDC]), loss by 2050 would be limited to 14,255 ha, versus 45,634 ha under a governance failure scenario (SC2) a divergence of 31,379 ha, equivalent to approximately 9.8% of the 2025 forest cover. These results provide a directly applicable quantitative baseline for revising the Kouilou Land Use Plan and updating the Congolese NDC reports. The main methodological limitations are the 30 m resolution of the Landsat imagery, which constrains detection of sub-pixel degradation, and the stationarity assumption of the Markov transition probabilities, which does not explicitly incorporate future climate-driven shifts in land-use pressure.

Mots-clés : Mayombe, remote sensing, modeling, Random Forest, deforestation, CA-Markov, land tenure, REDD+, forest fragmentation.

Résumé

Le district de Mvouti, situé dans le département du Kouilou (République du Congo), abrite une partie essentielle du massif forestier du Mayombe, qui englobe la réserve de biosphère de Dimonika (136 000 ha, UNESCO-MAB 1988). Cette réserve a été sélectionnée car elle représente un hotspot de biodiversité soumis à de fortes pressions anthropiques liées à l'orpaillage artisanal et à l'exploitation forestière. À partir de six composites d'images Landsat (2000–2025) classés via l'algorithme Random Forest sur Google Earth Engine, cet article quantifie la dynamique spatio-temporelle du couvert forestier, analyse la fragmentation du massif et simule trois trajectoires prospectives à l'horizon 2050 à l'aide de la modélisation CA-Markov. Avec une précision globale de classification de 90,6 % (κ moyen = 0,883), la forêt dense a perdu 32 106 ha (soit 9,1 % du couvert initial) entre 2000 et 2025. Le taux moyen de déforestation est estimé à 0,37 %/an, soit trois à quatre fois plus que la moyenne nationale congolaise. La désagrégation par statut foncier révèle des dynamiques contrastées : les zones situées hors des concessions forestières ont culminé à 2,27 %/an entre 2015 et 2020, tandis que les concessions aménagées (UAF) au sein de la zone tampon de la réserve ont maintenu des taux nettement inférieurs. La fragmentation s'est fortement intensifiée (le nombre de fragments est passé de 442 à 6 189 ; MESH : −21,5 %). Selon le scénario de gouvernance intégrée (SC3, conforme à la loi n° 33-2020 et à la Contribution Déterminée au niveau National [CDN]), les pertes d'ici 2050 se limitaient à 14 255 ha, contre 45 634 ha en cas de scénario de défaillance de la gouvernance (SC2). Ces résultats fournissent une base de référence quantitative directement applicable pour la révision du Plan d'Affectation des Terres du Kouilou et la mise à jour des rapports de la CDN congolaise.

Keywords: Mayombe, télédétection, modélisation, Random Forest, déforestation, CA-Markov, régime foncier, REDD+, fragmentation forestière.

*Corresponding author: Cédrick Belmich Nkoua Ondon, (cedrickbelmichondonnkoua@gmail.com). Tel. : (+243) 890431542

https://orcid.org/0009-0006-0289-293X; Received 25/08/2026; Revised 18/09/2026 ; Accepted 13/10/2026

DOI: https://doi.org/10.59228/rcst.026.v5.i4.361

Copyright: ©2026 Ondon et al. This is an open-access article distributed under the terms of the Creative Commons Attribution-NonCommercial-ShareAlike 4.0 International License (CC-BY-NC-SA 4.0), which permits unrestricted use, distribution, and reproduction in any medium, provided the original author and source are credited.

1. Introduction

The tropical forests of the Congo Basin constitute a natural heritage of inestimable value at the global scale. According to the 2025 Global Forest Resources Assessment, the Republic of the Congo possesses approximately 22.4 million hectares of forest, corresponding to a forest cover rate of 65% of its national territory, one of the highest in sub-Saharan Africa. These forest massifs store substantial quantities of carbon and play a determining role in regulating the regional hydrological cycle (FAO, 2025; Baccini et al., 2017; Harris et al., 2012).

The Mayombe, a mountainous forest massif extending continuously from Gabon to Angola (Cabinda) across the Republic of the Congo and the Democratic Republic of the Congo, constitutes one of the most diverse formations within this ensemble. In the Mvouti district, located within the Kouilou department of the Republic of the Congo, this massif harbors the Dimonika Biosphere Reserve (136,000 ha, UNESCO-MAB 1988, WDPA 13694), recognized for its exceptional biodiversity of primates, birds, and endemic plants.

Despite the protected status governing this reserve, the district's forest cover is subject to multiple and increasing anthropogenic pressures: shifting slash-and-burn agriculture, industrial logging, informal artisanal gold mining along watercourses, and expansion of the road network (Kimbatsa, 2021). A precise, spatially explicit assessment of these dynamics nevertheless remains limited for the Mvouti district. Available studies are restricted either to macro-regional or national estimates (CNREDD, 2018; Ickowitz et al.,2015; Megevand, 2013), or to point-based mapping that does not cover a temporal extent sufficient for prospective modeling (Potapov et al., 2012; Duveiller et al., 2008). More recent fine-scale assessments elsewhere in the Congo Basin, for instance around mining- and charcoal-driven fronts in south-eastern DRC, combine remote sensing with landscape-pattern analysis to link road and mining expansion to accelerated forest fragmentation (Khoji et al., 2023), yet no equivalent quantitative baseline exists for the Mayombe massif, despite recent field reports of expanding mining concessions in villages adjacent to Mvouti, such as Louvoulou in the neighboring Kakamoeka district (Africanews, 2026).

Thanks to multi-date imagery, satellite remote sensing now offers unique operational capabilities for addressing these gaps. The availability of Landsat archives since 2000 makes it possible to document a quarter-century of forest change at a 30 m spatial resolution, compatible with the requirements of national monitoring under the REDD+ mechanism (Hansen et al., 2013; Shapiro et al., 2021; Woodcock et al., 2008; Wulder et al., 2019). The use of the Google Earth Engine platform facilitates the processing of these massive image archives (Gorelick et al., 2017), while coupling with cellular automata and Markov chain models (CA-Markov) makes it possible to simulate future trajectories that differ according to land-use planning policies (Eastman, 2009; Kamusoko et al., 2013; Lusana et al., 2022; Tiye et al., 2025).

A simple diachronic analysis can only quantify past land-cover change between two or more observation dates; it cannot, by itself, anticipate how these trends might evolve under alternative policy or management conditions. The CA-Markov framework was therefore preferred because it combines a Markovian transition model, which projects the probability of change between land-cover states, with a cellular-automaton allocation rule, which distributes that change spatially according to neighborhood constraints. This dual structure allows (i) the explicit comparison of contrasting policy scenarios (business-as-usual, governance failure, integrated governance) and (ii) spatially explicit projections to 2050, both of which a purely retrospective diachronic analysis cannot provide.

Within this framework, this study aims to analyze past changes and model future dynamics of forest cover in the Mvouti district, in order to assess the effectiveness of different management statuses in addressing deforestation. Specifically, it pursues three objectives: (i) to map and quantify forest cover changes in the Mvouti district between 2000 and 2025; (ii) to analyze the spatial dynamics of deforestation and fragmentation in relation to land tenure status (Biosphere Reserve, managed concessions, unmanaged concessions); and (iii) to project three contrasting trajectories through 2050 to inform forest policy choices and the commitments of the Republic of the Congo's Nationally Determined Contribution (NDC).

2. Material and methods

2.1. Study Area

The Mvouti district is located in the southern part of the Republic of the Congo, within the Kouilou department, between latitudes 4°00' and 4°30' South, and longitudes 12°10' and 12°45' East. It covers a total area of approximately 366,000 hectares. The relief is characterized by the Mayombe mountain range, a succession of parallel ridges-oriented northwest–southeast, rising to 800 m in elevation on a Precambrian granitic and schisto-sandstone basement. Soils are predominantly ferrallitic, strongly leached, and acidic. The climate is humid tropical, strongly influenced by the cold Benguela marine current; annual rainfall exceeds 1,800 mm, with two marked dry seasons (July–August and January). The hydrographic network, particularly dense, is dominated by the watersheds of the Louboulou, Noumbi, and Loémé rivers.

Environmentally, the dominant vegetation is the semi-deciduous moist dense forest of the Mayombe, characterized by timber species of high commercial value (*Aucoumea klaineana*, *Terminalia superba*, *Entandrophragma* spp.). The forest fabric is strongly structured by two types of industrial activity: logging and mining (manganese, iron). Several forest concessions are currently under management planning (AFRIWOOD/NKOLA, ACI Louvakou, EMERSON-BOIS/BOUBISSI) or remain unmanaged (COFIBOIS, DOUMANGA), under ministerial orders No. 10821/2009, 710/2010, and 8692/2010 of the Congolese Ministry of Forest Economy (MEF). National Road 1 (RN1), which crosses the district from north to south, constitutes the principal driver of edge deforestation by facilitating access to the forest massifs. The Dimonika Biosphere Reserve occupies the northern part of the district and represents the major protected area within the study zone; it is nevertheless subject to strong anthropogenic pressures artisanal gold mining, shifting slash-and-burn agriculture, and illegal logging making it a privileged case study for analyzing forest dynamics under contrasting governance regimes.

Demographically, the district has approximately 20,000 inhabitants, predominantly rural, whose livelihoods rely largely on forest resources (hunting, gathering, and collection of non-timber forest products, artisanal logging). The main localities Mvouti, Londela-Kayes, and Nzambi are directly accessible from RN1. These biophysical and socio-economic characteristics make the Mvouti district a prime setting for analyzing the interactions between demographic pressure, land-use dynamics, and forest conservation in the tropical zone of Central Africa.

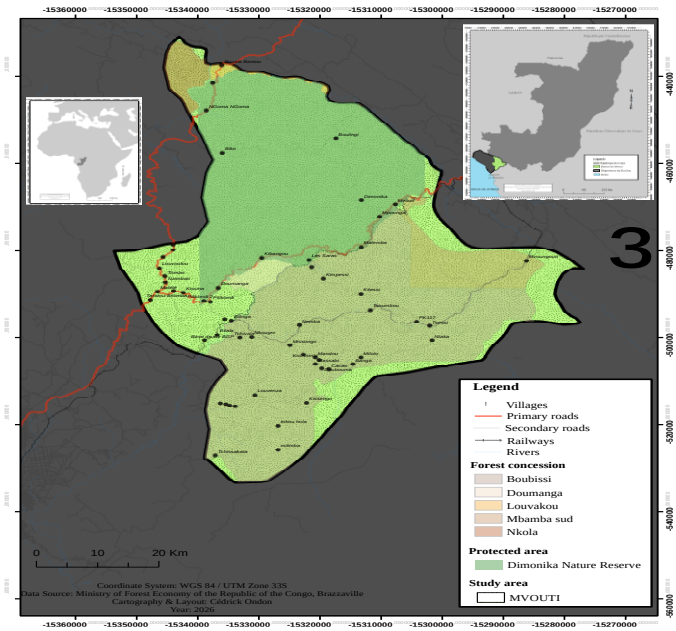

Figure 1. Geographic location of the Mvouti district within the Kouilou department, Republic of the Congo. Coordinate system: UTM zone 33 South (WGS 84).

2.2. Data acquisition and preprocessing

The analysis of land use and land cover (LULC) change is structured around six distinct, fixed historical milestones at five-year intervals: 2000, 2005, 2010, 2015, 2020, and 2025. To avoid multi-year temporal overlaps and ensure consistency across the 25-year study period, each milestone is anchored to a single, fixed nominal reference date set at the mid-year point (July 2nd) of the respective target year. The corresponding satellite datasets originate from the Landsat-5 (TM), Landsat-7 (ETM+), Landsat-8 (OLI/TIRS), and Landsat-9 (OLI-2/TIRS-2) missions, acquired and processed via the Google Earth Engine (GEE) platform. All selected Landsat scenes share a uniform 30 m spatial resolution, ensuring structural geometric consistency across missions over the entire study period. Atmospheric correction was applied upstream using the Collection 2 Level-2 Surface Reflectance products (the LEDAPS algorithm for Landsat 5/7 and the LaSRC algorithm for Landsat 8/9); Top-of-Atmosphere (TOA) products were explicitly excluded from all processing.

For each fixed reference year, image selection was restricted to the dry season the period corresponding to minimal cloud cover in the Mayombe region and strict filtering was applied at the scene level to retain exclusively imagery reporting less than 5%

cloud cover in its metadata. To ensure absolute radiometric comparability across the four sensor generations, Landsat 5 (TM) and Landsat 7 (ETM+) surface reflectance data were harmonized toward the spectral response of Landsat 8/9 (OLI) prior to final processing, following the band-specific linear transformation of Roy et al. (2016); native Landsat 8/9 reflectance data, which define the target spectral domain, were left unmodified.

Residual cloud, cloud shadow, cirrus, and dilated-cloud contamination were then rigorously removed at the pixel level using the QA_PIXEL quality band supplied with each Collection 2 Level-2 scene, whose cloud-detection algorithm derives from the CFmask method (Zhu & Woodcock, 2012). This pixel-level mask complements the scene-level filter by handling isolated, localized contamination. A robust temporal median reduction of the valid cloud-free pixels was then computed on GEE for each fixed target year. Unlike the arithmetic mean, the median is an estimator that effectively excludes residual extreme values caused by undetected clouds or cast shadows, thereby producing spectrally homogeneous, clear, and representative annual composite images for each reference year. To ensure the spatial integrity of the final products, the fraction of the study area reaching an adequate number of valid observations was verified at the pixel level, ensuring full and uniform coverage over the study area before entering the classification phase.

For visual analysis and sample collection, false-color near-infrared (NIR) composites were applied according to sensor specifications:

- Landsat 5 (TM) and Landsat 7 (ETM+): combination of the Near Infrared (B4), Red (B3), and Green (B2) bands.
- Landsat 8 (OLI) and Landsat 9 (OLI-2): combination of the Near Infrared (B5), Red (B4), and Green (B3) bands.

2.3. Land cover classification and binary reclassification

2.3.1. Multi-Class Supervised Classification

Multi-date LULC maps were produced through supervised classification using the Random Forest algorithm, recognized for its robustness with high-dimensional data and spectrally similar classes (Breiman, 2001; Rodriguez-Galiano et al., 2012; Noi & Kappas, 2018). The model was parameterized with an ensemble of 500 decision trees. The classifier was trained on five predictor variables per pixel: the near-infrared (NIR), first shortwave-infrared (SWIR1), and second shortwave-infrared (SWIR2) reflectance bands, together with the Normalized Difference Vegetation Index (NDVI) and the Normalized Difference Water Index (NDWI), computed for each annual composite on Google Earth Engine. Training and validation samples were split 80%/20% (`TRAINING_RATIO = 0.8`), and a fixed random seed (`seed = 42`) was used for both the train/test partition and the Random Forest classifier to ensure full reproducibility of the classification. The choice of these five variables reflects their recognized spectral complementarity for discriminating tropical land-cover states: NIR and NDVI capture vegetation vigor and canopy density, the SWIR bands are sensitive to canopy/soil moisture and woody structure, and NDWI isolates the hydrographic network.

Training samples were collected through assisted photo-interpretation on Google Earth Pro, based on a spatial stratification of the study area. Five thematic classes were retained (table I). To ensure the statistical representativeness of the model, the number of samples per class was defined proportionally to the visual extent of each stratum in the landscape: a strict minimum of 80 homogeneous polygons was digitized for minority classes, while dominant classes benefited from increased sampling effort.

Table I. Land use/land cover (LULC) class nomenclature and sampling structure

Code	LULC Class	Description	No. of Training Polygons	No. of Validation Points (per date)
1	Dense Forest	Primary or mature humid tropical forests of the Mayombe with closed canopy. High-biomass areas, preserved from direct human activity.	250	220
2	Degraded Forest	Secondary forests, post-logging regrowth, and disturbed forest edges. Includes old forest fallows.	180	110
3	Agricultural Zone	Active food crops (cassava, banana, market gardening) and recent grassy fallows. Mainly along RN1 and around villages.	120	85
4	Water	Local hydrographic network (perennial watercourses and water bodies).	80	25
5	Savanna / Bare Soil	Grassy and shrubby savannas, bare soil, dirt tracks, village settlements, quarries, and gold-panning sites.	110	60
	TOTAL		740	500

2.3.2. Binary reclassification protocol (Forest / Non-Forest)

Prior to assessing overall accuracy, a binary reclassification was performed to isolate strict forest dynamics. The Dense Forest class (code 1, tree cover ≥ 60%) was directly assigned to the "Forest" class (value 1). Conversely, all other classes including Degraded Forest (code 2, cover 30–59%), Agricultural Zone (code 3), Water (code 4), and Savanna / Bare Soil (code 5) were grouped under the "non-Forest" class (value 0), in accordance with Congo Basin MRV protocols (Hansen et al., 2013; Shapiro et al., 2021). Binary rasters were exported in GeoTIFF format (uint8, LZW compression) and reprojected into the UTM zone 33S (WGS 84) coordinate system. At this spatial resolution (30 m × 30 m), the elementary pixel area (Apix) is fixed at 0.09 ha. The consistency of this binarization was validated through cross-tabulation between the LULC maps and the resulting binary rasters.

2.4. Classification accuracy assessment

The validity of the multi-class and binary maps was independently verified through a stratified sampling protocol (Congalton & Green, 2009; Olofsson et al., 2014). For the LULC classification (5 classes): A total of 3,000 independent control points was distributed across the six dates (i.e., 500 points per annual map), allocated proportionally to the area of each stratum. For the binary classification (Forest / Non-Forest): A total of 1,800 independent control points was used (300 points per annual map). For each configuration, a confusion matrix was constructed to calculate the Overall Accuracy (OA), Cohen's Kappa coefficient (k), as well as Producer's Accuracy (PA) and User's Accuracy (UA), using the following formulas:

- Overall Accuracy (PG): $PG = \frac{\sum_{i=1}^{q} n_{ii}}{N}$ (1)

Where n_{ii} is the number of points correctly classified for class i, q is the number of classes, and N is the total number of validation samples.

- Kappa Coefficient (k) : $k = \frac{N\sum_{i=1}^{q} n_{ii} - \sum_{i=1}^{q}(n_{i+}\times n_{+i})}{N^2 - \sum_{i=1}^{q}(n_{i+}\times n_{+i})}$ (2)

Where n_{i+} is the row total i (total assigned to this class by the classifier) and n_{+i} is the column total i (actual total of ground-truth points for this class).

- Producer's Accuracy (PA_i): $PA_i = \frac{n_{ii}}{n_{+i}}$ (3) : and User's Accuracy (PU_i): $PU_i = \frac{n_{ii}}{n_{i+}}$ (4)

2.5. Analysis of forest dynamics

From the binary rasters, total forest area F_t (in hectares) was calculated for each date t by summing the pixels classified as "Forest," weighted by the unit pixel area (A_{pix}): $F_t = N_f(t) \times A_{pix}$ (5)

where $N_f(t)$ represents the total number of forest pixels identified on date t, and A_{pix} the elementary area of a 30 m pixel × 30 m, i.e., $A_{pix} = 0.09$ ha.

Absolute forest loss ΔF (in hectares) between two successive dates t and $t+1$ was obtained by difference: $\Delta F = F_t - F_{t+1}$ (6)

The annualized deforestation rate (in %/year), in accordance with FAO standards (FRA, 2020), was calculated using the following formula: $P = \frac{1}{n} \times \frac{F_t - F_{t+n}}{F_t} \times 100$ (7)

where n corresponds to the number of years within the period considered, with $n = 5$ for the five-year intervals. This linear formulation was adopted to ensure direct comparability with published national and regional reference values, notably those of the FAO (~0.10 for the Republic of the Congo) and CIFOR (~0.17). Rates were calculated for each of the five five-year periods and disaggregated by land tenure regime.

2.6. Forest fragmentation analysis

Forest fragmentation was assessed to quantify the spatial disaggregation of forest cover, following the approaches of McGarigal & Marks (1995) and Jaeger (2000). The analysis included the following metrics: (i) the number of patches (NP), obtained through connected-component analysis using **8-connectivity** (Moore neighborhood); (ii) the area of the largest patch; (iii) the mean and median areas of the remaining patches; and (iv) the effective mesh size (MESH), calculated as:

$$\text{MESH} = \frac{1}{A_{total}} \sum_{i} a_i^2 \qquad (8)$$

where a_i is the area of patch i and A_{total} is the total landscape area considered. The **splitting index** (SI) was also computed as:

s: $SI = \frac{A_{total}^2}{\sum_i a_i^2}$ (9)

where a value of 1 indicates an intact forest massif. Core forest was delineated by morphological erosion using a 3 × 3-pixel structuring element applied over three iterations, allowing the identification of interior forest located at least 90 m from the forest edge. In addition to these landscape-level metrics, four complementary FRAGSTATS-type indices reported in table X were calculated to characterize forest patch geometry in greater detail.

- Patch Density (PD) was defined as the number of forest patches per 100 ha of landscape:
- $PD = \frac{NP}{A_{total}} \times 100$ (10)
- Largest Patch Index (LPI) was calculated as the area of the largest forest patch expressed as a percentage of total forest area:
- $LPI = \frac{a_{max}}{A_{forest}} \times 100$ (11)
- Mean Patch Size (MPS) was obtained as the arithmetic mean area of all forest patches:
- $MPS = \frac{A_{forest}}{NP}$ (12)
- **Edge Density (ED)** was calculated as the total length of forest patch perimeter per unit landscape area, expressed in m/ha:

$$ED = \frac{\sum_i p_i}{A_{total}} \quad (13)$$

Where p_i is the perimeter of patch i. Finally, a pixel-by-pixel change map between 2000 and 2025 was produced, distinguishing four states: Stable Non-Forest (0 → 0), Stable Forest (1 → 1), Forest Gain (0 → 1), and Forest Loss (1 → 0).

2.7. Disaggregation of deforestation by Land tenure regime and temporal activation of concessions

Four land tenure zones, associated with distinct control regimes, were defined. The Dimonika Biosphere Reserve constitutes a maximum-priority protected area for conservation, registered under the UNESCO-MAB program (WDPA No. 13694). Managed concessions correspond to titles holding an active management plan, namely AFRIWOOD/NKOLA, ACI/LOUVAKOU, and EMERSON-BOIS/BOUBISSI. Unmanaged concessions group together areas exploited without an approved plan, such as COFIBOIS and DOUMANGA. Finally, the free zone corresponds to the remainder of the Mvouti district outside the concessions.

To avoid attributing to a concession deforestation that predates its legal existence, a temporal activation procedure was applied based on MEF orders No. 10821/2009, No. 710/2010, and No. 8692/2010. Accordingly, pixels belonging to land units not yet covered by a ministerial order at the date considered were reclassified into the free zone. Differences in forest dynamics between zones were then tested using the Kruskal-Wallis test, supplemented by pairwise Mann-Whitney comparisons, with a significance threshold set at $\alpha = 0.05$.

2.8. Binary CA-Markov modeling

The CA-Markov model was selected over alternatives (Land Change Modeler, CLUE-S, Dinamica EGO, or deep-learning-based allocators) due to its validated performance in African tropical forests, modest computational requirements, and alignment with Congolese REDD+ reporting scenarios. While intensive machine-learning methods were excluded, they are identified for future comparative analysis.

2.8.1. Transition Matrices

The modeling is based on transition matrices 2×2 constructed from historical binary rasters covering the 2000–2025 period. The transition probability P_{ij} from a state i to a state j is estimated by maximum likelihood from observed transitions. To standardize transition rates, these matrices were annualized using the t-th root method:

$$P_{ann} = P^{1/t} \quad (14)$$

Where t represents the duration, in years, of the observation period. The prospective Markovian process is then expressed as: $S_{t+1} = S_t \times P_{ann}$ (15)

2.8.2. Scenario Construction

Three prospective scenarios were constructed, each grounded in reference data or official Congolese policy guidance.

- SC1–Business-As-Usual (BAU): the matrix retained corresponds to the annualized probability estimated over the historical reference period. This scenario simulates the continuation of current anthropogenic and concessionaire practices in the region (Eastman, 2009; Tadese et al.,2021; Setiono et al., 2023).
- SC2–Governance Failure: the historical matrix is spatially amplified using the coefficients presented in table II. This scenario simulates the progressive abandonment of concession management specifications, the weakening of protected-area status, and the expansion of informal gold-panning or

charcoal-making activities (Kamusoko et al.,2013; Kleinschroth et al., 2019).

- SC3–Integrated Governance: the trend matrix is combined with a 48% reduction in the deforestation rate and a 48% increase in the regeneration rate, the latter capped at 5%/year. This 48% coefficient reflects the observed effectiveness of managed concessions in the Congo Basin (Tritsch et al., 2020; Kleinschroth et al., 2019), combined with strict application of Law No. 33-2020 (Art. 78), the National REDD+ Strategy (CNREDD, 2018), and the revised Nationally Determined Contribution (NDC, 2021).

Table II. Spatial coefficients aby land tenure regime and projection scenario

Scenario	α Dimonika (zone 1)	α Managed (zone 2)	α Unmanaged (zone 3)
SC1 – Business-As-Usual (BAU)	0.15	1.00	1.20
SC2 – Governance Failure	0.15	1.30	1.60
SC3 – Integrated Governance	0.05	0.40	0.70

2.8.3. Deforestation-potential surface and driving factors

The deforestation-potential layer P_"def,Sc" (x), used in the CA-Markov allocation, was derived through a systematic selection of driving factors. Several candidates (e.g., distance to mining/quarry sites, forest tracks, demographic variables) were initially considered but excluded due to weak correlation with observed forest loss ($p \geq 0.001$) or high multicollinearity (VIF > 10).

The final model retained five factors: elevation, slope, distance to roads, distance to localities, and distance to rivers. Distance to roads also captures forest tracks and mining-related access. All retained variables are significant (), directionally consistent with the literature (Kolb et al., 2013; Eastman, 2009), and show no multicollinearity (VIF < 10). These standardized layers were combined to produce , ensuring a robust and non-redundant basis for spatial allocation.

2.8.4. CA-Markov spatial simulation

The CA-Markov simulation combines the Markovian transition matrix, which determines the quantity of pixels to convert, with a cellular automaton mechanism, which determines the spatial location of conversions.

$$P = \begin{bmatrix} p_{11} & p_{12} & \cdots & p_{1m} \\ p_{21} & p_{22} & \cdots & p_{2m} \\ \vdots & \vdots & \ddots & \vdots \\ p_{m1} & p_{m2} & \cdots & p_{mm} \end{bmatrix}$$

Where p_{ij} represents the probability that class i will convert to class j over a given time step. At each annual step, the weighting of candidate pixels combines deforestation potential with a contagion effect: $w_{conv}(x) = 0.60 \times P_{def,sc}(x) + 0.40 \times V_{NF}(x)$

where $V_{NF}^{(x)}$ is the proportion of non-forest pixels within a 9×9-pixel neighborhood centered on x (270 m). The simulation is repeated annually from 2025 to 2050 (25 steps) with a fixed random seed (seed = 42) to ensure reproducibility.

2.9. Validation of the CA-Markov model

Validation follows a temporal split-sample protocol (calibration: 2000–2015; validation: 2015–2020), consistent with Pontius *et al.*, (2008) and Pontius & Millones (2011). The main metric is the Figure of Merit (FoM), with an acceptable threshold of FoM > 10–15% (Pontius & Millones, 2011; Lusana et al., 2022). The Quantity/Allocation decomposition makes it possible to distinguish quantity errors (volume of pixels lost) from allocation errors (location of losses). The logical consistency of the scenarios is verified through the condition: SC2 < SC1 < SC3 (2050 losses).

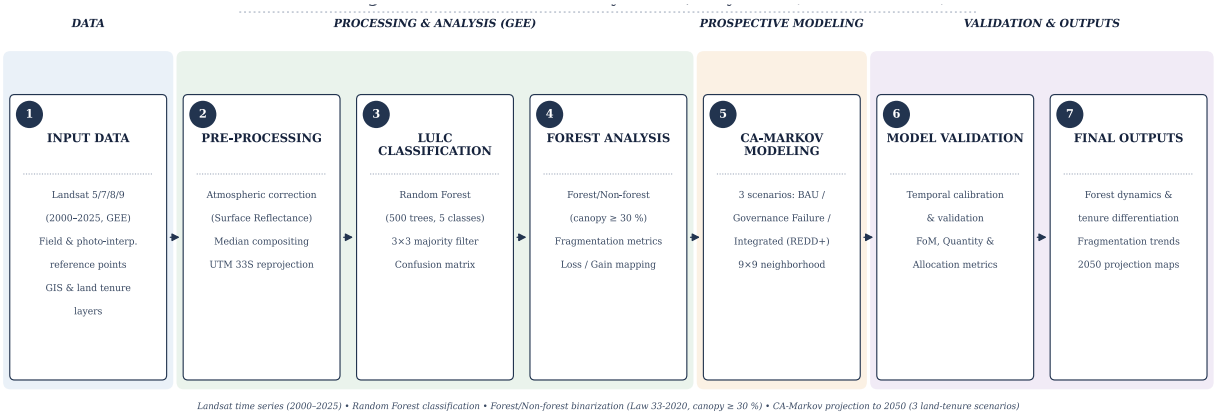

Figure 2. Conceptual diagram of LULC data processing and CA-Markov simulation of deforestation scenarios through 2050

3. Results

3.1. Land Use/Land Cover (LULC) Change, 2000–2025

The multi-date supervised classification reveals a significant transformation of land cover in the Mvouti district over the 2000–2025 period (). Dense forest, the dominant class, declined from 351,596 ha (96.1% of the territory) in 2000 to 319,490 ha (87.4%) in 2025, a net loss of 32,106 ha over twenty-five years. In parallel, degraded forest increased continuously (from 1,840 ha [0.5%] to 32,964 ha [9.0%]), reflecting the intensification of logging pressure. Agricultural areas expanded moderately (from 716 ha to 2,514 ha). Savannas and bare soils recorded a slight contraction (from 11,531 ha to 10,705 ha), which may be attributable to spontaneous vegetation recolonization or partial conversion to degraded forest that is spectrally difficult to distinguish. The LULC maps (figure 3) show that deforestation is concentrated primarily along the RN1 corridor and near village centers, consistent with edge-deforestation patterns documented in the Congo Basin (Geist & Lambin, 2002; Kleinschroth et al., 2019).

Table III. LULC area changes in the Mvouti district (2000–2025), in hectares

LULC Class	2000 (ha)	2005 (ha)	2010 (ha)	2015 (ha)	2020 (ha)	2025 (ha)
Dense Forest	351,596	345,038	341,912	332,896	322,436	319,490
Degraded Forest	1,840	7,562	10,508	18,336	29,562	32,964
Agricultural Zone	716	1,339	1,587	2,810	2,643	2,514
Water	75	79	79	78	84	84
Savanna / Bare Soil	11,531	11,740	11,671	11,636	11,032	10,705

Table IV. Gross gain, loss, swap, and net change per LULC class

Class	Area_t1_ha	Area_t2_ha	Gain_ha	Loss_ha	Net_change_ha	Swap_ha	Absolute_change_ha	Period
Dense forest	351595,5	345037,9	40,6	6598,1	-6557,6	81,1	6638,7	2000_2005
Degraded forest	1840,4	7561,6	5725,5	4,3	5721,3	8,6	5729,8	2000_2005
Agricultural area	716,4	1338,6	706,8	84,6	622,2	169,2	791,4	2000_2005
Water	74,6	79,4	5	0,3	4,7	0,5	5,3	2000_2005
Bare soil/Savanna	11530,5	11740	277,6	68,1	209,4	136,2	345,7	2000_2005
Dense forest	345037,9	341912,5	70	3195,4	-3125,4	140	3265,4	2005_2010
Degraded forest	7561,6	10507,8	2988,7	42,5	2946,1	85,1	3031,2	2005_2010
Agricultural area	1338,6	1586,7	344,3	96,2	248,1	192,4	440,5	2005_2010
Water	79,4	79,3	0,2	0,3	-0,1	0,4	0,4	2005_2010
Bare soil/Savanna	11740	11671,2	93,8	162,5	-68,7	187,6	256,3	2005_2010
Dense forest	341912,5	332896,1	102,1	9118,5	-9016,5	204,2	9220,6	2010_2015
Degraded forest	10507,8	18336,4	8232,3	403,6	7828,7	807,3	8635,9	2010_2015
Agricultural area	1586,7	2810,3	1394,5	170,8	1223,6	341,7	1565,3	2010_2015
Water	79,3	78,4	0,4	1,2	-0,9	0,7	1,6	2010_2015
Bare soil/Savanna	11671,2	11636,3	235,4	270,3	-35	470,8	505,7	2010_2015
Dense forest	332896,1	322435,7	160,1	10620,5	-10460,3	320,3	10780,6	2015_2020
Degraded forest	18336,4	29562,4	11571,8	345,8	11226	691,5	11917,6	2015_2020
Agricultural area	2810,3	2642,7	879,4	1047	-167,6	1758,8	1926,4	2015_2020
Water	78,4	84,3	7,4	1,5	5,9	3	8,9	2015_2020
Bare soil/Savanna	11636,3	11032,3	127,7	731,7	-604	255,4	859,3	2015_2020
Dense forest	322435,7	319490,4	58,8	3004,1	-2945,3	117,5	3062,8	2020_2025
Degraded forest	29562,4	32964	3558,8	157,2	3401,6	314,4	3715,9	2020_2025
Agricultural area	2642,7	2514	480,8	609,6	-128,7	961,7	1090,4	2020_2025
Water	84,3	83,6	0,1	0,7	-0,6	0,2	0,8	2020_2025
Bare soil/Savanna	11032,3	10705,4	62,4	389,3	-326,9	124,8	451,7	2020_2025

Table IV shows that the 31,123.6-ha gain recorded for Degraded Forest accounts for 96.9% of the 32,105.1-ha net loss of Dense Forest. In other words, the “deforestation” measured in this study is almost entirely a process of canopy degradation (Dense → Degraded), rather than a direct conversion to agriculture or another land use the net gain in Agricultural Area (+1,797.6 ha) and the net loss to

Savanna/Bare Soil (−825.1 ha, likely a transitional stage) together account for a much smaller share of the overall dynamic. This distinction, discussed further in section 4.1, has direct implications for the management levers most relevant to curbing forest loss in Mvouti.

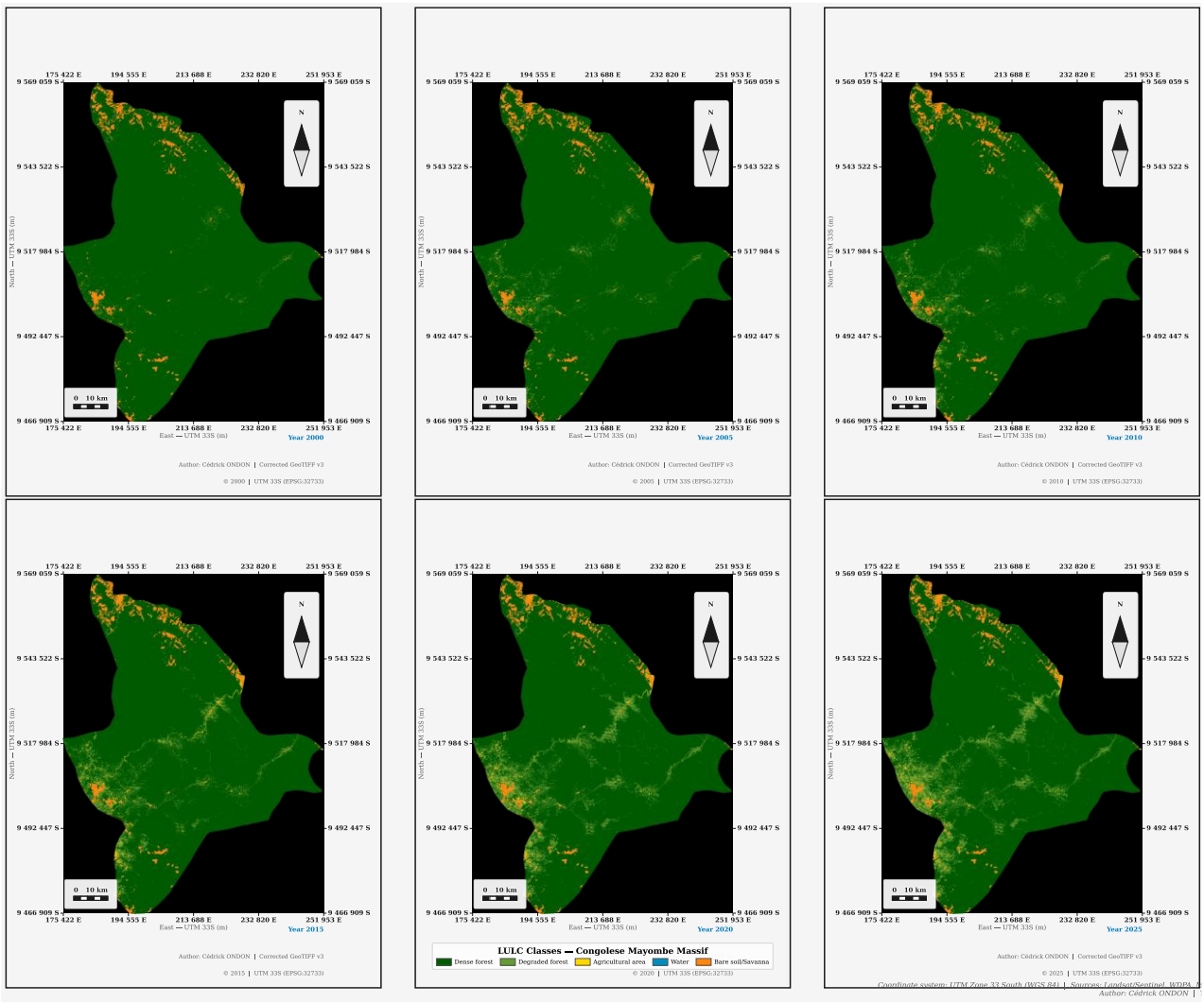

Figure 3. Land use/land cover (LULC) maps of the Mvouti district for the six dates (2000–2025). Coordinate system: UTM zone 33 South (WGS 84)

3.2. Classification accuracy

The accuracy of five-class LULC classifications was assessed by stratified random sampling (N = 500 points per date, totaling 3,000 points), with reference labels assigned by manual visual interpretation performed independently by the author and co-authors on Google Earth Pro historical imagery, matched to each classification date. The mean overall accuracy (Eq. 1) is 90.6% (κ = 0.883), above the CNREDD standard (OA ≥ 85%, κ ≥ 0.80). For the binary Forest/Non-Forest classification (N = 300 points per date, 1,800 total; same reference points reclassified into binary categories), the mean overall accuracy reaches 93.3% (κ = 0.866), consistent with the CNREDD Congo standard of 90% (Ouissika & Milandou, 2019). The main confusion concerns transitions between Degraded Forest and Dense Forest in the presence of residual cloud cover (Defourny et al., 2017; Li et al., 2020).

Table V. Producer's Accuracy (PA), User's Accuracy (UA) and F1-score by LULC class and date

Year	LULC Class	PA (%)	UA (%)	F1 (%)	OA / κ (year)
2000	Dense Forest	92	90.2	91.09	90.4 / 0.880
2000	Degraded Forest	78	85.71	81.67	
2000	Agricultural Zone	93	93.94	93.47	
2000	Water	95	100	97.44	
2000	Savanna/Bare Soil	94	83.19	88.27	
2005	Dense Forest	92	91.09	91.54	90.6 / 0.883
2005	Degraded Forest	79	85.87	82.29	
2005	Agricultural Zone	93	93.94	93.47	
2005	Water	95	100	97.44	
2005	Savanna/Bare Soil	94	83.19	88.27	
2010	Dense Forest	92	92.93	92.46	91.0 / 0.888
2010	Degraded Forest	81	86.17	83.51	
2010	Agricultural Zone	93	93.94	93.47	
2010	Water	95	100	97.44	
2010	Savanna/Bare Soil	94	83.19	88.27	
2015	Dense Forest	92	92	92	90.8 / 0.885
2015	Degraded Forest	80	86.02	82.9	
2015	Agricultural Zone	93	93.94	93.47	
2015	Water	95	100	97.44	
2015	Savanna/Bare Soil	94	83.19	88.27	
2020	Dense Forest	92	91.09	91.54	90.6 / 0.883
2020	Degraded Forest	79	85.87	82.29	
2020	Agricultural Zone	93	93.94	93.47	
2020	Water	95	100	97.44	
2020	Savanna/Bare Soil	94	83.19	88.27	
2025	Dense Forest	92	90.2	91.09	90.4 / 0.880
2025	Degraded Forest	78	85.71	81.67	
2025	Agricultural Zone	93	93.94	93.47	
2025	Water	95	100	97.44	
2025	Savanna/Bare Soil	94	83.19	88.27	

Table VI. Accuracy of binary Forest/Non-Forest classifications (2000–2025)

Year	N pts (bin.)	OA bin. (%)	κ (bin.)
2000	300	93.3	0.867
2005	300	93.7	0.873
2010	300	94.0	0.880
2015	300	94.7	0.893
2020	300	93.0	0.860
2025	300	91.0	0.820
Mean	—	93.3	0.866

3.2. Binary Forest dynamics and deforestation rates

Analysis of annualized rates per five-year period (FAO method, Eq. 7, table VII) reveals a nonlinear dynamic in forest cover change. The highest rates are observed for the 2010–2015 and 2015–2020 periods, at 0.527%/year and 0.628%/year respectively, values above the national average (≈0.10%/year) (FAO, 2025) and CIFOR estimates (≈0.17%/year). The 2020–2025 period shows a markedly lower rate (0.183%/year), close to the level observed for the 2005–2010 period.

Table VII. Annualized deforestation rates per five-year period (FAO method)

Period	Duration (years)	Forest t1 (ha)	Forest t2 (ha)	Loss (ha)	Rate (%/year)
2000–2005	5	351,596	345,038	6,558	0.373
2005–2010	5	345,038	341,912	3,125	0.181
2010–2015	5	341,912	332,896	9,016	0.527
2015–2020	5	332,896	322,436	10,460	0.628
2020–2025	5	322,436	319,490	2,945	0.183

Forest/non-forest class areas were also adjusted following the approach of Olofsson et al. (2014), based on the confusion matrix, to account for thematic classification uncertainty. Table VIII presents, for each date, the mapped (raw) areas, the adjusted areas, and their associated standard errors and 95% confidence intervals.

Table VIII. Adjusted areas of the forest/non-forest classes and associated confidence intervals (Olofsson et al., 2014 method).

Year	Class	N (samples)	Mapped area (ha)	Adjusted area (ha)	SE (ha)	95% CI lower (ha)	95% CI upper (ha)
2000	Non-forest (0)	150	14,161.9	31,780.7	6,479.8	19,080.3	44,481.1
2000	Forest (1)	150	351,595.5	333,976.7	6,479.8	321,276.3	346,677.1
2005	Non-forest (0)	150	20,719.5	42,478.8	7,062.4	28,636.5	56,321.2
2005	Forest (1)	150	345,037.9	323,278.6	7,062.4	309,436.2	337,121.0
2010	Non-forest (0)	150	23,844.9	38,052.2	5,930.0	26,429.4	49,675.0
2010	Forest (1)	150	341,912.5	327,705.2	5,930.0	316,082.4	339,328.0
2015	Non-forest (0)	150	32,861.4	48,863.2	6,157.7	36,794.1	60,932.3
2015	Forest (1)	150	332,896.1	316,894.2	6,157.7	304,825.1	328,963.3
2020	Non-forest (0)	150	43,321.7	64,078.9	6,942.6	50,471.4	77,686.4
2020	Forest (1)	150	322,435.7	301,678.6	6,942.6	288,071.1	315,286.1
2025	Non-forest (0)	150	46,267.0	74,514.7	7,919.1	58,993.2	90,036.2
2025	Forest (1)	150	319,490.4	291,242.7	7,919.1	275,721.2	306,764.3

Adjusted areas for the non-forest class are consistently higher than the corresponding mapped (raw) areas at every date in the time series. The 95% confidence intervals do not overlap between the two classes at any date considered.

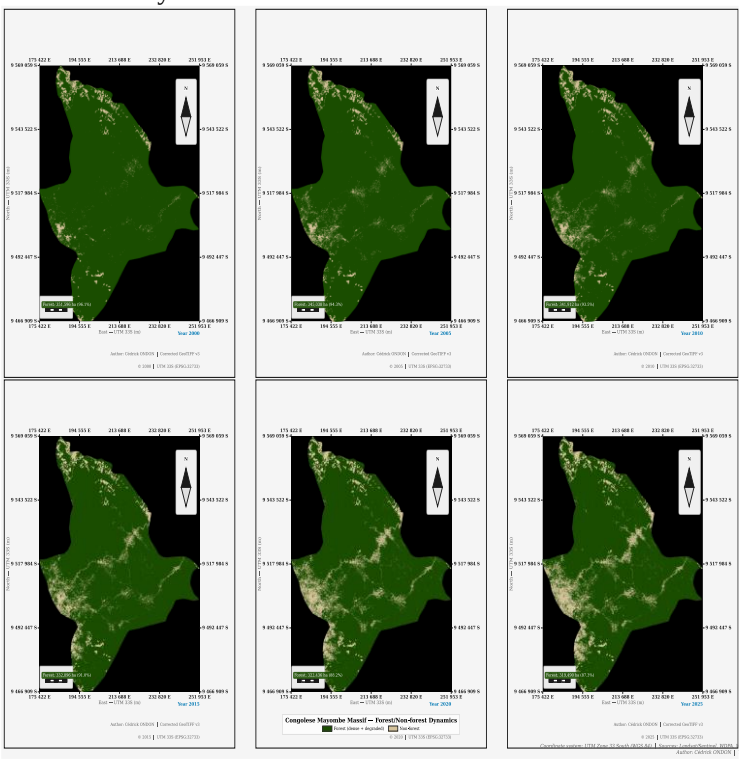

Figure 4. Binary forest cover dynamics (Forest/Non-Forest) 2000–2025 according to the Congolese national definition (Law No. 33-2020)

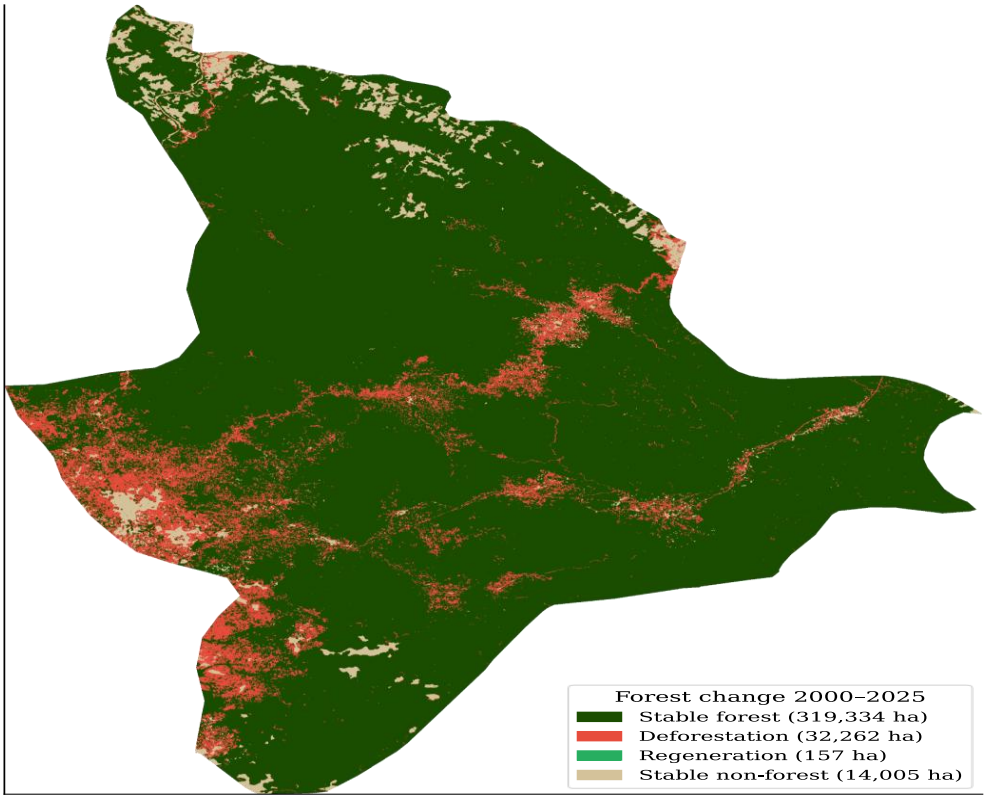

Figure 5. Forest change map between 2000 and 2025: stable pixels, forest gains, and forest losses

3.3. Deforestation disaggregated by land tenure regime

Disaggregation by land tenure regime (table IX) reveals sharply contrasting dynamics. The Dimonika Biosphere Reserve (Zone 1) records persistent but contained deforestation (0.079–0.309%/year), constituting regulatory violations under the UNESCO-MAB status. Unmanaged concessions (Zone 3) exhibit the most variable rates, reaching 0.831%/year during 2015–2020. The free zone (Zone 0) consistently records the highest rates in absolute and relative terms, with a peak of 2.270%/year during 2015–2020, reflecting the scale of informal pressure outside any regulatory framework.

Table IX. Annualized deforestation rates (%/year) disaggregated by land tenure regime and period

Period	Zone 0 Free	Zone 1 Dimonika	Zone 2 Managed	Zone 3 Unmanaged	Overall Status
2000–2005	1.435	0.188	0.347	0.379	Concerning
2005–2010	0.603	0.079	0.212	0.141	Moderate
2010–2015	1.797	0.229	0.538	0.662	Critical
2015–2020	2.270	0.309	0.600	0.831	Critical
2020–2025	0.852	0.089	0.123	0.354	Improving

Differences in forestation rate between land tenure zones were tested using the non-parametric Kruskal-Walli's test (Rate_% by zone, n = 4-6 dates per zone), given the small per-zone sample size and non-normality of rate distributions. The test is significant ($H = 8.012$, $p = 0.046$, $\alpha = 0.05$), confirming that land tenure regime is associated with significant differences in forest cover trajectory. Pairwise Mann-Whitney U post-hoc comparisons show that only Managed versus Unmanaged concessions differ significantly ($p = 0.029$); no other pairwise comparison reaches significance, including Dimonika versus Managed ($p = 0.067$, borderline).

The significance of the binary Forest/Non-Forest change between each pair of consecutive dates was additionally tested pixel-by-pixel with McNemar's test on the paired classified maps. All five five-year transitions, as well as the overall 2000–2025 change, are highly significant (χ^2 from 31,765 to 113,833; $p < 1 \times 10{-}300$ in every case), confirming that the observed loss of forest pixels is not attributable to random classification noise. Accuracy-adjusted area estimates and their 95% confidence intervals (Olofsson et al., 2014) using the stratified accuracy-assessment sample, N = 150 points per class per date) show that the two study endpoints differ significantly: adjusted forest area is 333,977 ha (95% CI: 321,276–346,677) in 2000 versus 291,243 ha (95% CI: 275,721–306,764) in 2025,

non-overlapping intervals confirming a robust net loss over the full period. At the finer scale of individual five-year intervals, however, sampling uncertainty is larger relative to the shorter time span: the 95% confidence interval of the adjusted annual rate includes zero for all five sub-periods, so no single five-year interval can be distinguished from the others with statistical confidence at this sample size, even though the cumulative 25-year trend is unambiguous.

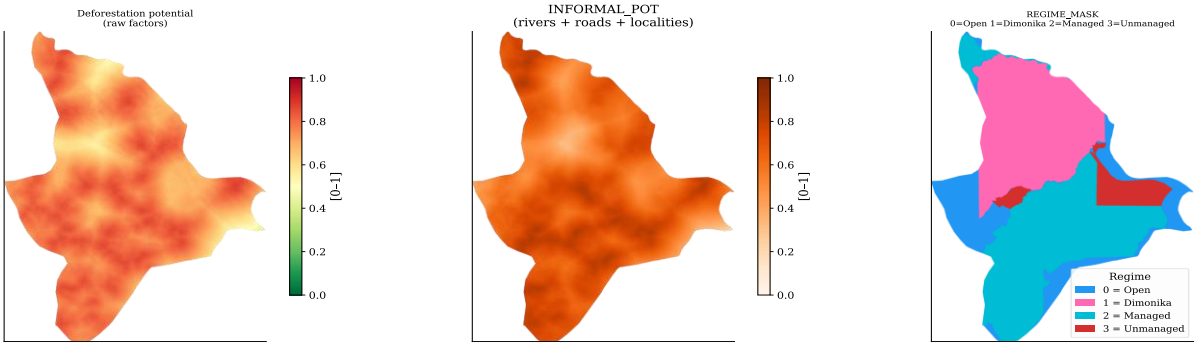

Figure 6. Map of deforestation potential and land tenure regimes in the Mvouti district

3.4. Forest cover fragmentation

Fragmentation analysis (table X) reveals a continuous increase in the spatial disaggregation of the forest massif. The number of patches increased from 442 in 2000 to 6,189 in 2025, representing a more than 14-fold increase over twenty-five years. In parallel, patch density (PD, Eq. 10) rose from 0.121 to 1.692 patches per 100 ha. The Largest Patch Index (LPI, Eq. 11) declined from 96.02% to 86.05%, indicating that, although the dominant forest block still accounts for most of the remaining forest cover, its relative share of the landscape decreased by nearly 10 percentage points. Mean Patch Size (MPS, Eq. 12) fell sharply from 795.46 ha to 51.62 ha, corresponding to a 15-fold reduction, while Edge Density (ED, Eq. 13) nearly quadrupled, from 8.15 m/ha to 31.33 m/ha, reflecting an increasingly convoluted forest–non-forest boundary. The Effective Mesh Size (MESH, Eq. 8) decreased from 337,156 ha to 264,837 ha, a decline of 21.5%, whereas the Splitting Index (SI, Eq. 9) increased slightly from 1.00 to 1.05, indicating a modest increase in landscape fragmentation over the period.

Table X. Forest fragmentation metrics, Mvouti district (2000–2025)

Year	NP	PD (/100 ha)	LPI (%)	MPS (ha)	ED (m/ha)	MESH (ha)	SI
2000	442	0.121	96.02	795.46	8.15	337,156	1.00
2005	877	0.240	94.19	393.43	15.07	323,887	1.00
2010	1,324	0.362	93.28	258.24	18.23	317,325	1.01
2015	2,941	0.804	90.54	113.19	25.15	295,976	1.02
2020	5,376	1.470	87.07	59.98	30.55	272,896	1.04
2025	6,189	1.692	86.05	51.62	31.33	264,837	1.05

3.6. CA-Markov model validation and 2050 projections

The CA-Markov model validation, based on calibration over the 2000–2015 period and simulation for 2015–2020, demonstrates overall satisfactory performance. The Figure of Merit (FoM) reaches 11.0% (overall FoM = 10.8%), which falls within the acceptable range of 10–15% commonly reported for CA-Markov applications in African tropical forest contexts at 30 m resolution (Pontius & Millones, 2011; Lusana et al., 2022).

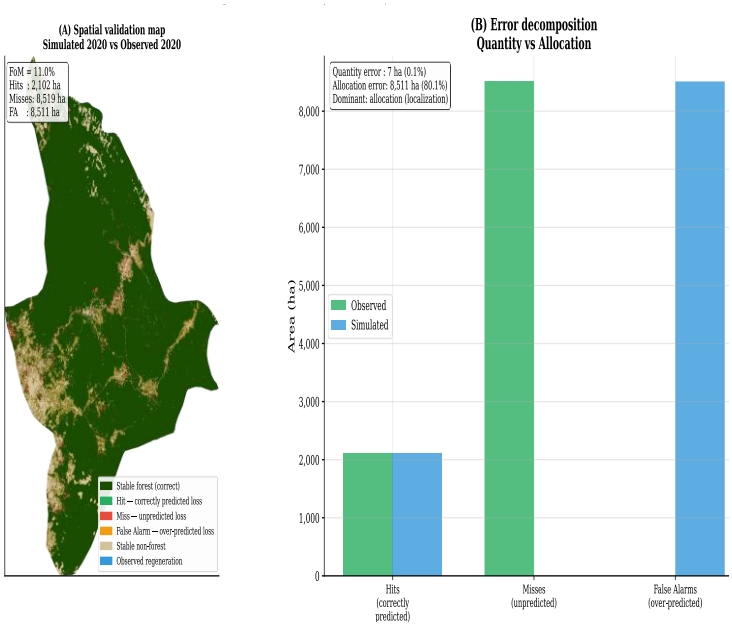

Figure 7. *Spatial validation map(A), error decomposition (B)*

Error analysis reveals a negligible quantity error (7.5 ha, representing 0.1% of total cover), while the dominant source of error is spatial allocation (8,511 ha, or 80.1%), consistent with expected behavior for CA-Markov models at this resolution. The overall accuracy reaches 95.3%, with a Cohen's Kappa coefficient (Eq. 2) of 0.77, indicating strong agreement between observed and simulated maps. The logical consistency among scenarios is confirmed (SC2 < SC1 < SC3).

3.7. 2050 projections

The three prospective scenarios through 2050 generate strongly divergent trajectories (table XI; figure 8). Under SC1 (BAU), forest cover reaches 291,200 ha (79.6%), representing a loss of 28,290 ha. Under SC2 (governance failure), forest cover falls to 273,857 ha (74.9%, loss of 45,634 ha). Under SC3 (integrated governance), forest cover is maintained at 305,235 ha (83.4%, loss limited to 14,255 ha). The gap between SC2 and SC3 by 2050 amounts to 31,379 ha, equivalent to approximately 9.8% of current cover.

Table XI. Projected forest areas through 2050 under the three CA-Markov scenarios

Scenario	Forest 2050 (ha)	Forest 2050 (%)	ΔForest (ha)	% Cover 2025
SC1 – Business-As-Usual (BAU)	291,200	79.6 %	−28,290	91.1 %
SC2 – Governance Failure	273,857	74.9 %	−45,634	85.7 %
SC3 – Integrated Governance (Law 33-2020)	305,235	83.4 %	−14,255	95.5 %

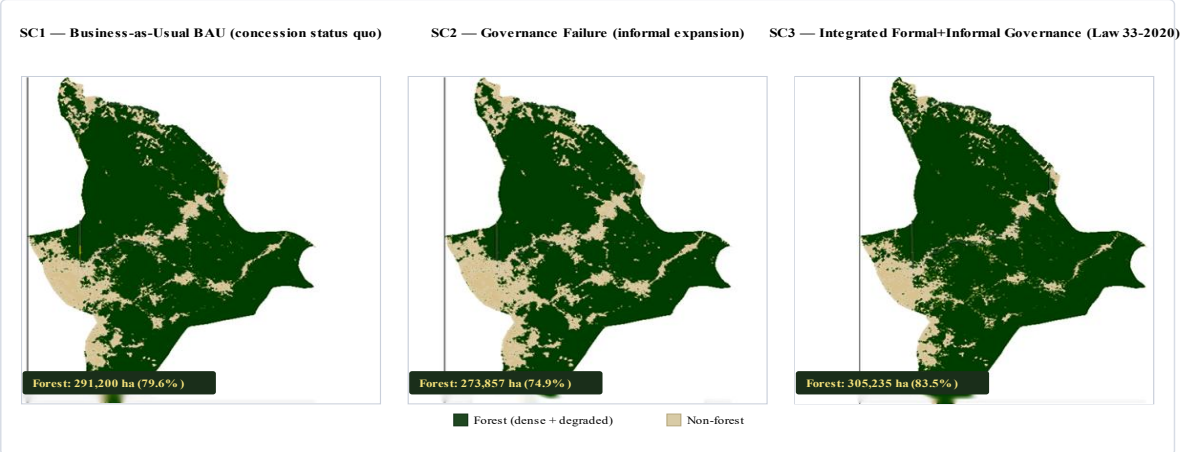

Figure 8. CA-Markov projections of forest cover through 2050 under the three scenarios (SC1 – BAU, SC2 – Governance Failure, SC3 – Integrated Governance)

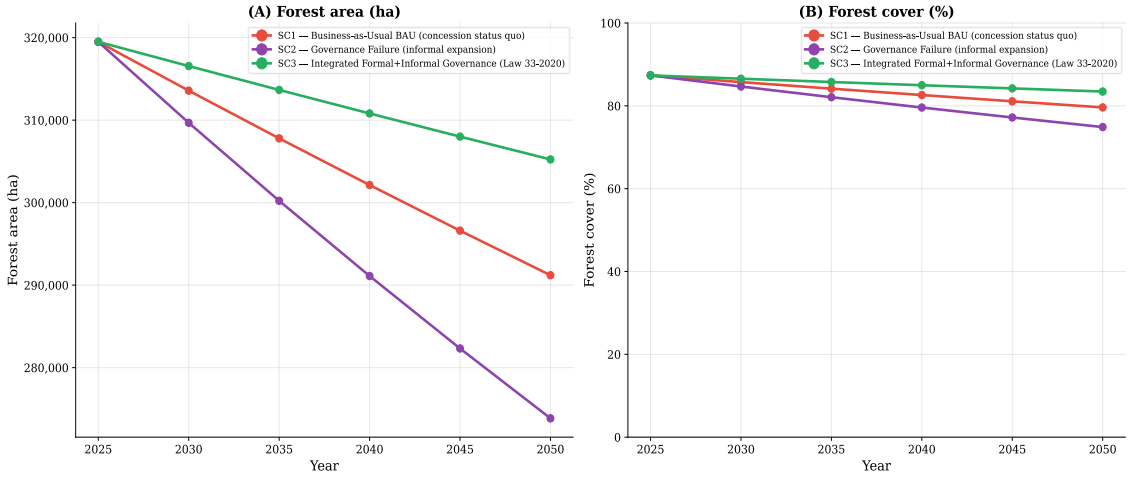

Figure 9. Complete forest cover trajectory 2000–2050

The detailed temporal evolution (table XII) further supports these differentiated dynamics. Scenario SC1 shows a steady and gradual decline in forest cover between 2030 and 2050. Scenario SC2 exhibits a more rapid and continuous deforestation trend, reflecting the effects of unregulated informal expansion. In contrast, SC3 shows a slower and more controlled decline, highlighting the relative effectiveness of integrated governance combining formal regulation and local practices.

Table XII. Temporal evolution of forest cover (ha and %) from 2030 to 2050 under scenarios SC1 (Business-as-Usual), SC2 (Governance Failure), and SC3 (Integrated Governance)

Scenario	Year	Forest_ha	Forest_%
SC1 Business-as-Usual BAU (concession status quo)	2030	313574,2	85,73
SC1 Business-as-Usual BAU (concession status quo)	2035	307789,9	84,15
SC1 Business-as-Usual BAU (concession status quo)	2040	302134,9	82,61
SC1 Business-as-Usual BAU (concession status quo)	2045	296605,9	81,09
SC1 Business-as-Usual BAU (concession status quo)	2050	291200,4	79,62
SC2 Governance Failure (informal expansion)	2030	309678,4	84,67
SC2 Governance Failure (informal expansion)	2035	300221,6	82,08
SC2 Governance Failure (informal expansion)	2040	291107,3	79,59
SC2 Governance Failure (informal expansion)	2045	282322,8	77,19
SC2 Governance Failure (informal expansion)	2050	273856,5	74,87
SC3 Integrated Formal+Informal Governance (Law 33-2020)	2030	316553,5	86,55
SC3 Integrated Formal+Informal Governance (Law 33-2020)	2035	313660,2	85,76
SC3 Integrated Formal+Informal Governance (Law 33-2020)	2040	310809,8	84,98
SC3 Integrated Formal+Informal Governance (Law 33-2020)	2045	308001,8	84,21
SC3 Integrated Formal+Informal Governance (Law 33-2020)	2050	305235,3	83,45

4. Discussion

The results obtained for the Mvouti district confirm regional dynamics observed across the Congo Basin, while revealing important local specificities. We discuss successively: (i) the magnitude and kinetics of deforestation, (ii) the explanatory factors of its spatial distribution, (iii) the significance of the observed fragmentation, (iv) the methodological strengths and limitations, (v) the policy implications of the 2050 projections, and (vi) a comparison with studies from the Congo Basin and other African regions.

4.1. Magnitude and kinetics of deforestation

Building on early continental assessments that first quantified deforestation rates across the world's humid tropical forests from satellite data (Achard et al., 2002), the mean deforestation rate over 2000–2025 (0.37%/year) is markedly higher than national FAO estimates (0.06%/year for the Republic of Congo, 2010–2020; FAO, cited by CAFI, 2024) and CIFOR assessments for the Congo Basin as a whole (0.17%/year, 2000–2005; Tchatchou et al., 2015). This divergence reflects the intensification of local pressures in the Mvouti district, linked to the presence of industrial logging concessions and the rise of artisanal gold mining. These results are consistent with work showing the heightened vulnerability of border and roadside forest areas to anthropogenic pressures, as new disturbance fronts emerge at the periphery of the basin (Biswas et al., 2025), and the structuring effect of logging concessions on deforestation in the Congo Basin (Houngbedji et al., 2026).

The nonlinear dynamics of deforestation rates is particularly informative.

The acceleration observed between 2010 and 2020 (peaks of 0.53 and 0.63%/year) coincides with the extension of the secondary road network in Kouilou (RN1 and access tracks to concessions) and the rise of artisanal gold mining, whose indirect impact on deforestation can be several times greater than its direct footprint: in eastern DRC, indirect deforestation linked to artisanal mining (agricultural expansion and settlement growth around mining sites) has been estimated at up to 28 times the area directly cleared for the extraction itself (Ladewig et al., 2024). The marked slowdown between 2020 and 2025 (0.18%/year) must be interpreted with caution: it could reflect a positive effect of the entry into force of Law No. 33-2020, but post-2025 data will be needed to distinguish this legal effect from interannual climatic variability affecting satellite detection.

A key finding, highlighted in table IV (section 3.1), is that the net loss of dense forest does not mainly correspond to a direct conversion to agriculture or settled areas (the net gain in agricultural land, +1,797.6 ha, is an order of magnitude lower than the loss of dense forest), but is almost entirely absorbed by a gain in degraded forest (+31,123.6 ha, 96.9% of the net loss of dense forest). This indicates that the dominant process in Mvouti is a progressive degradation of canopy structure, consistent with selective and informal logging rather than with agricultural expansion. This pattern echoes continental-scale evidence that timber extraction and forest degradation, rather than outright conversion, account for a large share of tropical forest loss (Curtis et al., 2018), and it illustrates the practical difficulty of separating degradation from deforestation within global climate-reporting definitions (Sasaki & Putz, 2009). It also contrasts with the smallholder-clearing-dominated pattern documented across the wider Congo Basin (Tyukavina et al., 2018), suggesting that Mvouti's

trajectory is shaped more by concession-linked selective logging than by the shifting agriculture that dominates elsewhere in the basin. This distinction matters for policy: in landscapes dominated by degradation, the management levers (controlling the intensity of selective logging, regulating sawing, enforcing buffer zones) differ from those needed to limit agricultural expansion. Priority should therefore go to interventions targeting informal and selective logging practices, rather than to simply containing agriculture. In this respect, reduced-impact logging techniques have been shown to substantially lower selective-logging emissions in the Congo Basin without necessarily reducing timber yields, offering a concrete, degradation-focused lever directly applicable to Mvouti's concessions (Umunay et al., 2019).

4.2. Spatial factors of deforestation and the role of land tenure regimes

Disaggregation by land tenure regime confirms the central hypothesis of our protocol: deforestation rates are significantly differentiated according to land protection and management status. Areas outside concessions (Zone 0), lacking any formal regulatory framework, systematically show the highest rates (up to 2.27%/year in 2015–2020), underscoring the absence of effective control mechanisms on informal pioneer fronts. Concessions under an active management plan (Zone 2) show more stable and lower rates, consistent with two independent studies showing a substantial reduction in deforestation in concessions with an approved management plan in the Congo Basin: a first quasi-experimental evaluation over the 2000–2010 period estimated 74% lower deforestation in concessions with an approved management plan compared with similar concessions without one (Tritsch et al., 2020). A more recent causal evaluation, covering five Congo Basin countries (Cameroon, CAR, DRC, RC, Gabon) over the 2000–2020 period, estimates that concessions with a validated management plan lose on average 47% less forest cover per year than comparable concessions without a plan, with an effect that persists up to 19 years after validation (Houngbedji et al., 2026). These two studies, although methodologically distinct and covering different time windows, converge on the same qualitative finding and reinforce the policy relevance of accelerating management-plan validation in Mvouti's unmanaged concessions (COFIBOIS, DOUMANGA).

The persistence of deforestation in the Dimonika Biosphere Reserve (Zone 1), although contained (0.08–0.31%/year), constitutes a documented violation of its UNESCO-MAB protected status. It is mainly explained by the pressure of artisanal gold mining along waterways and by localized agricultural encroachment, confirming the limited surveillance capacity of ACFAP in formally protected areas. Spearman correlation analysis identifies elevation, distance to roads, distance to settlements, distance to waterways, and slope as significant factors ($p < 0.001$), with directions consistent with the classic theoretical models of proximate and underlying causes of tropical deforestation, which distinguish agricultural expansion, timber extraction, and infrastructure development as proximate causes, driven by underlying economic, demographic, institutional, and technological factors (Geist & Lambin, 2002). The absence of problematic multicollinearity (VIF < 10) ensures the robustness of the weight assigned to these factors in the CA-Markov simulation.

4.3. Fragmentation and ecological implications

The increase in patch count from 442 to 6,189 over twenty-five years, combined with the reduction of MESH from 337,156 ha to 264,837 ha (−21.5%), indicates growing but still moderate fragmentation, relative to the size of the massif, within the range documented across the wider Congo Basin using comparable landscape metrics (Riitters et al., 2000; Jaeger, 2000), and consistent with global evidence that even moderate increases in patch density can accelerate carbon losses at newly created forest edges (Brinck et al., 2017). A comparable magnitude of fragmentation, similarly attributed to the expansion of mining- and logging-related road networks, has recently been documented elsewhere in the Congo Basin, where the largest-patch index of natural forest fell markedly under sustained road and mining pressure (Khoji Muteya et al., 2023; Mpanda et al., 2022). The largest patch, still exceeding 311,000 ha, ensures baseline connectivity for wide-ranging species (great apes, large mammals), but the reduction of core forest from 92.1% to 81.1% of cover is concerning for interior-forest species. The increase in the splitting index from 1.00 to 1.05 confirms that the forest remains dominated by a single major block, but that the spatial fragmentation process has begun and has accelerated since 2015. This reduction in core forest is particularly critical for the primates and large mammals recorded in the Dimonika Reserve, a concern reinforced by broader evidence that habitat fragmentation, independent of outright habitat loss, exerts lasting negative effects on biodiversity and ecosystem functioning (Haddad et al., 2015; Wilson et al., 2016), and that even nominally protected tropical

forest areas can experience biodiversity collapse when edge effects and human pressure accumulate (Laurance et al., 2012).

4.4. Methodological strengths and limitations

Several methodological choices strengthen the reliability of the results. The choice of the CA-Markov framework, rather than alternatives (Land Change Modeler, CLUE-S, Dinamica EGO, or deep-learning-based allocators), is justified by its well-established validation framework (Figure of Merit), its modest data requirements, and the direct interpretability of its transition matrices for REDD+ MRV reporting. The stratified accuracy-assessment protocol, applied consistently across the six dates, provides area estimates with explicit confidence intervals. Dating concessions by their legal date of establishment avoids retrospectively attributing pre-existing deforestation to concessions that did not yet exist.

Several limitations must be noted. The 30 m spatial resolution of the Landsat archive, essential to cover a 25-year series, limits the detection of sub-pixel degradation and may therefore under-estimate early degradation processes. The CA-Markov framework assumes stationarity of transition probabilities within each scenario; it does not explicitly incorporate future climatic changes in agricultural or mining pressure, nor discontinuous political shocks. As already noted in section 4.1, the marked slowdown of 2020–2025 cannot yet be attributed with certainty to Law No. 33-2020 rather than to climatic variability; post-2025 monitoring is needed. Alternative models better suited to non-stationary or highly nonlinear dynamics (Dinamica EGO, CLUE-S, deep-learning allocators) were not compared with CA-Markov in this study; a recent systematic review of CA-Markov applications confirms that model choice remains a recognized source of uncertainty in LULC projections (Setiono et al., 2023), and such a comparison would be useful to characterize the sensitivity of the 2050 projections to the choice of modeling framework.

4.5. Policy implications of the 2050 scenarios

The 31,379-ha divergence between the Governance Failure (SC2) and Integrated Governance (SC3) trajectories by 2050 equivalent to about 9.8% of the district's 2025 forest cover represents a substantial and policy-relevant margin. In carbon terms, using reference aboveground biomass values for Mayombe dense forest (395.7 Mg ha^{-1} on average for intact African forests and close to 429 Mg ha^{-1} for the Congo Basin; Lewis et al., 2013), which are consistent with local estimates obtained in the DRC portion of the Mayombe massif (Michel et al., 2022), this margin corresponds to a non-negligible avoided loss of carbon stock, in addition to the habitat preserved for the primate and bird species associated with the biodiversity of the Dimonika Reserve. Achieving the SC3 trajectory rather than drifting toward SC2 depends on operational levers already available to the Congolese forest administration:

the effective finalization and implementation of management plans for the AFRIWOOD/NKOLA and ACI Louvakou concessions and EMERSON-BOIS/BOUBISSI; bringing the currently unmanaged COFIBOIS and DOUMANGA concessions under an approved management plan; strict application of Article 78 of Law No. 33-2020 on buffer zones around protected areas; and operationalizing the forest-monitoring commitments of the revised Nationally Determined Contribution (NDC, 2021) at the district scale, using the present LULC time series as a reference. As noted in §4.4, these scenario trajectories remain conditional projections rather than forecasts: they assume stationary transition dynamics within each governance regime and do not anticipate exogenous shocks (commodity price changes affecting mining pressure, shifts in regional food demand, or climate-related changes in agricultural viability). The SC1–SC3 comparison should therefore be interpreted as an exercise in bounding a range of plausible 2050 outcomes under different levels of governance, rather than as a single most-likely trajectory.

4.6. Comparison with regional and pan-African studies

To situate the Mvouti results within the broader literature, we compared them with nine studies selected for their geographic or methodological proximity, at three levels: three studies within the Mayombe massif itself (RC, DRC, Angola), four at the Congo Basin scale (Cameroon, Gabon, CAR, and multi-country syntheses), and two studies from other African tropical forest contexts using comparable Random Forest and/or CA-Markov approaches (Ethiopia, Nigeria). Table XII summarizes this comparison in terms of period, method, deforestation rate, and main factors.

Within the Mayombe massif, the divergence in deforestation intensity is striking. The mean rate documented for Mvouti (0.37%/year, 2000–2025) is more than three times higher than that reported for the

Cabinda component of the massif in Angola (~0.11%/year, 1986–2019), based on a comparable Landsat/MODIS satellite monitoring approach (Fernandez & Granja-Martins, 2020). This gap is consistent with the relative integrity maintained by the Cabinda block of the Mayombe, where decades of armed conflict reduced resource-extraction pressures compared with the Congolese and DRC sides of the massif, an effect only recently reversed by post-2018 urban expansion and the lifting of logging concession suspensions. In the DRC, a comparison of land-use regimes in the Luki Biosphere Reserve area documents a similar gradient between high/moderate-use zones and low-use zones in terms of tree diversity and carbon storage loss (Michel et al., 2022), paralleling our own zonal contrast between unmanaged concessions (Zone 0) and actively managed concessions (Zone 2), reinforcing an explanation of deforestation intensity based on land tenure regime rather than purely biophysical factors.

At the Congo Basin scale, the factors identified for Mvouti closely align with those reported elsewhere. In Gabon, CAR, and four other Congo Basin countries, a recent national sample-based inventory by Shapiro et al. (2026) likewise attributes most forest loss to small-scale agriculture and artisanal or industrial logging, and finds deforestation broadly stable at the basin scale over 2015–2023 while degradation expands, a trend broadly consistent with the plateau we document for 2020–2025, although our data point to a genuine deceleration rather than mere stability. Using a methodological chain directly comparable to ours (Random Forest classification in Google Earth Engine combined with a Markov chain projection in IDRISI/TerrSet), Yuh et al. (2024) estimate dense-forest loss at the Congo Basin scale equivalent to about 0.52%, 0.12%, and 0.21% per year over 1990–2000, 2000–2010, and 2010–2020 respectively, rates of the same order as, but generally lower than, those observed in Mvouti, consistent with the Mvouti district functioning as a more heavily pressured national sub-front, exposed to concessions and mining, rather than a basin-wide average. This is corroborated at the concession scale by Houngbedji et al. (2026) across five Congo Basin countries including Gabon, and by Cameroonian evidence from Debus et al. (2024, 2025) on factors linked to logging-road expansion.

Outside the Congo Basin, two studies using comparable Random Forest/CA-Markov approaches in ecologically distinct African tropical forest contexts help delineate which of our findings are basin-specific versus more broadly generalizable. In the Majang Forest Biosphere Reserve in southwestern Ethiopia, Tadese et al. (2021) used an identical CA-Markov/IDRISI framework and documented a far more severe loss of forest land of 77.8% between 1987 and 2017, mainly due to small-scale agricultural expansion in a densely populated agrarian frontier, a rate an order of magnitude higher than our estimate. This underscores that the relatively moderate deforestation observed in Mvouti reflects a still-low population density and the persistence, albeit imperfect, of concession-based land-use control specific to the Congolese Mayombe, rather than a generic African pattern. In the Oban Division of Cross River National Park in Nigeria, within the Upper Guinean forest block of West Africa, Fitz et al. (2022) documented increasing fragmentation between 2000 and 2020 using landscape pattern metrics directly comparable to those calculated in §4.3, attributing it mainly to agricultural encroachment and the limited effectiveness of protected-area management, a pattern that mirrors, in a different biogeographic context, our own finding of persistent management-related leakage in the nominally protected Dimonika Biosphere Reserve. Taken together, this comparison across the Mayombe massif, the wider Congo Basin, and two other African tropical forest contexts confirms that the factors and spatial patterns identified for Mvouti road- and mining-linked pioneer fronts, differential effectiveness of concession management, and incomplete protection of biosphere reserves are broadly consistent with the regional literature, while situating Mvouti on a gradient of anthropogenic pressure shaped primarily by land tenure regime and conflict history rather than by climatic or biophysical factors alone.

5. Conclusion

This study provides a methodologically rigorous and empirically grounded contribution to the understanding of the spatio-temporal dynamics of forest cover in the Congolese Mayombe within the Mvouti district, covering a quarter-century (2000–2025) at the 30 m Landsat resolution. Four principal scientific contributions can be identified.

First, it establishes that dense forest in the Mvouti district lost 32,106 ha (9.1% of its initial cover) between 2000 and 2025, with a mean deforestation rate (0.37%/year) three to four times higher than the Congolese national average. The dynamic is nonlinear, with peaks during 2010–2020 and a slowdown in 2020–2025 whose causal attribution requires

confirmation through post-2025 data (effect of Law No. 33-2020 versus climatic variability).

Second, spatial disaggregation by land tenure regime reveals that areas outside concessions and unmanaged concessions concentrate the bulk of deforestation pressure, while concessions under effective management significantly reduce their rates, confirming the effectiveness of certified forest management tools in the Congo Basin. The deforestation documented within the Dimonika Biosphere Reserve signals the inadequacy of current protected-area monitoring capacity.

Third, CA-Markov projections through 2050 quantify the decision-making challenge: depending on whether Congolese forest policy maintains the status quo (SC1: −28,290 ha), experiences governance failure (SC2: −45,634 ha), or fully implements its legal framework and REDD+ commitments (SC3: −14,255 ha), trajectories diverge by 31,379 ha by 2050, equivalent to nearly 10% of current cover. These projections constitute a directly applicable quantitative baseline for revising the Kouilou Territorial Planning and Management Plan and for the biennial update reports of the Congolese NDC.

Fourth, rigorous validation at every stage of the processing chain (OA ≥ 90.4% for LULC maps, OA ≥ 91.0% for binary maps, FoM = 11.0% for CA-Markov) guarantees the reliability of the results within the MRV standards of the REDD+ mechanism.

These results call for a three-pronged policy response: strengthening surveillance capacity in the Dimonika Biosphere Reserve (ACFAP equipment, anti-poaching and anti-gold-panning patrols); accelerating the development of management plans for unmanaged forest concessions (COFIBOIS, DOUMANGA) in compliance with Article 78 of Law No. 33-2020; and developing sustainable economic alternatives for local communities to reduce agricultural pressure on forest edges (agroforestry, valorization of non-timber forest.

Data and code availability

The Google Earth Engine classification script and the Python CA-Markov modeling/validation code developed for this study are publicly available under the MIT license at https://github.com/cedrick14/Mayombe-LULC-AMarkov2/tree/main/Mayombe_LULC_CAMarkov_Reproducible

Acknowledgments

The authors thank the deanery of the Faculty of Agronomic Sciences and Environment and the Department of Natural Resource Management at the University of Kinshasa for their institutional, logistical, administrative, and scientific support within the Master's Program in Geomatics and Climate Change. They also thank the Ministry of Forest Economy of the Republic of the Congo for providing concession and land-tenure data, and the Centre de Recherche sur la Durabilité et la Productivité des Plantations Industrielles (CRDPI) and the Congo Basin Water Resources Research and Capacity-Building Center (CRREBaC) for their scientific contributions and exchanges

Funding

This research was conducted within the Master's Program in Geomatics and Climate Change, under a scholarship granted through the Climate Smart Agrifood Systems (CSAS) Project.

Conflict of Interest

The authors declare no conflicts of interest.

Ethical Considerations

This research was conducted in accordance with the fundamental ethical principles of scientific research.

Contribution of the authors

C.B.N.O.: Conceptualization, methodology, and writing of the original draft.

J.H.T.T.: Data collection.

J.O.A.: Data collection.

M.O.O.: Manuscript review and editing.

P.-C.B.B.: Manuscript review and editing.

R.M.T.: Supervision.

A.P.L.M.: Data collection; manuscript review and editing.

R.V.K.: Supervision.

B.N.L.: Supervision.

E.L.L.: Conceptualization, methodology, and writing of the original draft; manuscript review and editing.

ORCID

Ondon N.C.B.: https://orcid.org/0009-0004-1945-689X;

Tsoala T. J.H.: https://orcid.org/0009-0006-0289-293X;

Abedi O.J.: https://orcid.org/0009-0006-5390-4865;
Opelele O.M.: https://orcid.org/0000-0003-3712-8940;
Bolaluembe B. P.-C.: https://orcid.org/0000-0001-9848-838X;
Tshimanga M.R. : https://orcid.org/0000-0002-4726-3495;
Kizungu V.R.: https://orcid.org/0000-0002-1051-6890
LeLe N.B. : https://orcid.org/0009-0007-0427-1130;
Lutete L.E.: https://orcid.org/0000-0002-1584-7592.

References

Achard, F., Eva, H. D., Stibig, H.-J., Mayaux, P., Gallego, J., Richards, T., & Malingreau, J.-P. (2002). Determination of deforestation rates of the world's humid tropical forests. *Science, 297*(5583), 999–1002.

Africanews. (2026, May 4). *Bassin du Congo : Des forêts détruites par le chevauchement des activités humaines*. https://fr.africanews.com/2026/05/04/bassin-du-congo-des-forets-detruites-par-le-chevauchement-des-activites-humaines/

Baccini, A., Walker, W., Carvalho, L., Farina, M., Sulla-Menashe, D., & Houghton, R. A. (2017). Tropical forests are a net carbon source based on aboveground measurements of gain and loss. *Science, 358*(6360), 230–234.

Biswas, S., Kleinschroth, F., Mayaux, P., Bourgoin, C., Ernst, C., Verhegghen, A., & Vancutsem, C. (2025). Increasing forest disturbance in the Congo Basin is driven by an emerging frontier in Cameroon. *Earth's Future, 13*(4), e2024EF005613. https://doi.org/10.1029/2024EF005613

Breiman, L. (2001). Random forests. *Machine Learning, 45*(1), 5–32.

Brinck, K., Fischer, R., Groeneveld, J., Lehmann, S., Dantas De Paula, M., Pütz, S., Sexton, J. O., Song, D., & Huth, A. (2017). High resolution analysis of tropical forest fragmentation and its impact on the global carbon cycle. *Nature Communications*, 8(1), 14855. https://doi.org/10.1038/ncomms14855

BRLI/MEF. (2014). *Plan d'aménagement du territoire du Kouilou 2014–2024*. Ministère de l'Économie Forestière.

Central African Forest Initiative. (2024). *Republic of Congo country page*. https://cafi.org/country/republic-of-congo/

CNREDD. (2018). *Niveau d'émission de référence pour les forêts de la République du Congo*. Ministère du Développement Durable.

Congalton, R. G., & Green, K. (2009). *Assessing the accuracy of remotely sensed data: Principles and practices* (2nd ed.). CRC Press.

Curtis, P. G., Slay, C. M., Harris, N. L., Tyukavina, A., & Hansen, M. C. (2018). Classifying drivers of global forest loss. *Science, 361*(6407), 1108–1111.

Debus, A., Beauchamp, E., Acworth, J., Ewolo, A., Kamga, J., Verhegghen, A., Zébazé, C., & Lines, E. R. (2024). A labelled dataset to classify direct deforestation drivers from Earth Observation imagery in Cameroon. *Scientific Data, 11*(1), 564. https://doi.org/10.1038/s41597-024-03384-z

Debus, A., Beauchamp, E., Kamga, J., Verhegghen, A., Zébazé, C., & Lines, E. R. (2025). Evaluating satellite data and deep learning for identifying direct deforestation drivers in Cameroon. *Remote Sensing Applications: Society and Environment, 39*, 101653. https://doi.org/10.1016/j.rsase.2025.101653

Duveiller, G., Defourny, P., Desclée, B., & Mayaux, P. (2008). Deforestation in Central Africa: Estimates at regional, national and landscape levels by advanced processing of systematically distributed Landsat extracts. *Remote Sensing of Environment, 112*(5), 1969–1981.

Eastman, J. R. (2009). *IDRISI Taiga: Guide to GIS and image processing* (Version 16.02). Clark Labs, Clark University.

Food and Agriculture Organization of the United Nations. (2020). *Global forest resources assessment 2020: Main report*.

Food and Agriculture Organization of the United Nations. (2025). *Global forest resources assessment 2025*.

Fernandez, H. M., Gomes, C. P., & Martins, F. M. G. (2020). Monitorização por satélite da desflorestação da floresta do Maiombe em Cabinda, Angola nos últimos 33 anos. *Revista GEAMA, 6*(3), 81–91.

Fitz, J., Adenle, A. A., & Speranza, C. I. (2022). Increasing signs of forest fragmentation in the Cross River National Park in Nigeria: Underlying drivers and need for sustainable responses. *Ecological Indicators, 139*, 108943. https://doi.org/10.1016/j.ecolind.2022.108943

Geist, H. J., & Lambin, E. F. (2002). Proximate causes and underlying driving forces of tropical deforestation. *BioScience, 52*(2), 143–150.

Gorelick, N., Hancher, M., Dixon, M., Ilyushchenko, S., Thau, D., & Moore, R. (2017). Google Earth Engine: Planetary-scale geospatial analysis for everyone. *Remote Sensing of Environment, 202*, 18–27.

Haddad, N. M., Brudvig, L. A., Clobert, J., Davies, K. F., Gonzalez, A., Holt, R. D., Lovejoy, T. E., Sexton, J. O., Austin, M. P., Collins, C. D., Cook,

W. M., Damschen, E. I., Ewers, R. M., Foster, B. L., Jenkins, C. N., King, A. J., Laurance, W. F., Levey, D. J., Margules, C. R., … Townshend, J. R. (2015). Habitat fragmentation and its lasting impact on Earth's ecosystems. *Science Advances*, 1(2), e1500052. https://doi.org/10.1126/sciadv.1500052

Hansen, M. C., Potapov, P. V., Moore, R., Hancher, M., Turubanova, S. A., Tyukavina, A., Thau, D., Stehman, S. V., Goetz, S. J., Loveland, T. R., Kommareddy, A., Egorov, A., Chini, L., Justice, C. O., & Townshend, J. R. G. (2013). High-resolution global maps of 21st-century forest cover change. *Science*, 342(6160), 850–853. https://doi.org/10.1126/science.1244693

Harris, N. L., Brown, S., Hagen, S. C., Saatchi, S. S., Petrova, S., Salas, W., Hansen, M. C., Potapov, P. V., & Lotsch, A. (2012). Baseline map of carbon emissions from deforestation in tropical regions. *Science*, 336(6088), 1573–1576. https://doi.org/10.1126/science.1217962

Houngbedji, K., Bouvier, M., Leblois, A., Makak, J.-S., & Mertens, B. (2026). Forest management plan validation gradually reduces forest loss in Congo Basin concessions. *Communications Earth & Environment*, *7*, 414. https://doi.org/10.1038/s43247-026-03429-8

Ickowitz, A., Powell, B., Salim, M. A., & Sunderland, T. C. H. (2015). Forests, trees, and micronutrient-rich food consumption in sub-Saharan Africa. *PLOS ONE*, *10*(4), e0136579.

Jaeger, J. A. G. (2000). Landscape division, splitting index, and effective mesh size: New measures of landscape fragmentation. *Landscape Ecology*, *15*(2), 115–130.

JGI, & MEFE, République du Congo. (2010). *Sondages de biodiversité et socio-économiques dans la Réserve de Biosphère de Dimonika*. MEFE.

Kamusoko, C., Aniya, M., Adi, B., & Manjoro, M. (2009). Rural sustainability under threat in Zimbabwe – Simulation of future land use/cover changes in the Bindura district based on the Markov-cellular automata model. Applied Geography, 29(3), 435–447. https://doi.org/10.1016/j.apgeog.2008.10.002

Khoji Muteya, H., N'tambwe Nghonda, D.-D., Kalenda, F. M., Strammer, H., Kankumbi, F. M., Malaisse, F., Bastin, J.-F., Sikuzani, Y. U., & Bogaert, J. (2023). Mapping and quantification of miombo deforestation in the Lubumbashi charcoal production basin (DR Congo): Spatial extent and changes between 1990 and 2022. *Land*, *12*(10), 1852. https://doi.org/10.3390/land12101852

Kimbatsa, F. G. (2020). L'impact écologique des activités humaines sur la biodiversité dans la réserve de la biosphère de Dimonika dans le Mayombe (République du Congo). *Espace Géographique et Société Marocaine*, 36, 150–174. https://doi.org/10.34874/IMIST.PRSM/EGSM/21679

Kleinschroth, F., Healey, J. R., Sist, P., Mortier, F., & Gourlet-Fleury, S. (2019). Road expansion and persistence in forests of the Congo Basin. *Nature Sustainability*, *2*, 628–634.

Kolb, M., Mas, J.-F., & Galicia, L. (2013). Evaluating drivers of land-use change and transition potential models in a complex landscape in Southern Mexico. *International Journal of Geographical Information Science*, *27*(9), 1804–1827. https://doi.org/10.1080/13658816.2013.770517

Ladewig, M., Angelsen, A., Masolele, R. N., & Chervier, C. (2024). Deforestation triggered by artisanal mining in eastern Democratic Republic of the Congo. *Nature Sustainability*, *7*(11), 1452–1460. https://doi.org/10.1038/s41893-024-01421-8

Lambin, E. F., Geist, H. J., & Lepers, E. (2003). Dynamics of land-use and land-cover change in tropical regions. *Annual Review of Environment and Resources*, *28*, 205–241.

Lambin, E. F., Turner, B. L., Geist, H. J., Agbola, S. B., Angelsen, A., Bruce, J. W., Coomes, O. T., Dirzo, R., Fischer, G., Folke, C., George, P. S., Homewood, K., Imbernon, J., Leemans, R., Li, X., Moran, E. F., Mortimore, M., Ramakrishnan, P. S., Richards, J. F., … Xu, J. (2001). The causes of land-use and land-cover change: Moving beyond the myths. *Global Environmental Change*, 11(4), 261–269. https://doi.org/10.1016/S0959-3780(01)00007-3

Laurance, W. F., Useche, D. C., Rendeiro, J., Kalka, M., Bradshaw, C. J. A., Sloan, S. P., Laurance, S. G., Campbell, M., Abernethy, K., Alvarez, P., Arroyo-Rodriguez, V., Ashton, P., Benítez-Malvido, J., Blom, A., Bobo, K. S., Cannon, C. H., Cao, M., Carroll, R., Chapman, C., … Zamzani, F. (2012). Averting biodiversity collapse in tropical forest protected areas. *Nature*, 489(7415), 290–294. https://doi.org/10.1038/nature11318

Lewis, S. L., Sonké, B., Sunderland, T., Begne, S. K., Lopez-Gonzalez, G., van der Heijden, G. M. F., Phillips, O. L., Affum-Baffoe, K., Baker, T. R., Banin, L., Bastin, J.-F., Beeckman, H., Boeckx, P., Bogaert, J., De Cannière, C., Chezeaux, E., Clark, C. J., Collins, M., Djagbletey, G., … Zemagho, L. (2013). Above-ground biomass and structure of 260 African tropical forests. *Philosophical Transactions of the Royal Society B: Biological Sciences*, 368(1625), 20120295. https://doi.org/10.1098/rstb.2012.0295

Li, W., Dong, R., Fu, H., Wang, J., Yu, L., & Gong, P. (2020). Integrating Google Earth imagery with

Landsat data to improve 30-m resolution land cover mapping. *Remote Sensing of Environment, 237*, 111563.

Lusana, B., Munyemba, F., Kafuti, C., Ndjele, L., & Herold, M. (2022). Scenario-based land use/land cover change assessment in Katanga using CA-Markov model. *Remote Sensing Applications: Society and Environment, 28*, 100838.

McGarigal, K., & Marks, B. J. (1995). *FRAGSTATS: Spatial pattern analysis program for quantifying landscape structure* (General Technical Report PNW-GTR-351). USDA Forest Service.

Megevand, C. (2013). *Deforestation trends in the Congo Basin: Reconciling economic growth and forest protection*. World Bank.

Michel, O. O., Yu, Y., Fan, W., Lubalega, T., Chen, C., & Sudi Kaiko, C. K. (2022). Impact of land use change on tree diversity and aboveground carbon storage in the Mayombe tropical forest of the Democratic Republic of Congo. *Land, 11*(6), 787.

Mpanda Mukenza, M., Khoji Muteya, H., N'Tambwe Nghonda, D.-D., Sambiéni, K. R., Malaisse, F., Cabala Kaleba, S., Bogaert, J., & Useni Sikuzani, Y. (2022). Uncontrolled exploitation of *Pterocarpus tinctorius* Welw. and associated landscape dynamics in the Kasenga Territory: Case of the rural area of Kasomeno (DR Congo). *Land, 11*(9), 1541. https://doi.org/10.3390/land11091541

Noi, P. T., & Kappas, M. (2018). Comparison of random forest, k-nearest neighbor, and support vector machine classifiers for land cover classification using Sentinel-2 imagery. *Sensors, 18*(1), 18.

Olofsson, P., Foody, G. M., Herold, M., Stehman, S. V., Woodcock, C. E., & Wulder, M. A. (2014). Good practices for estimating area and assessing accuracy of land change. *Remote Sensing of Environment, 148*, 42–57.

Ouissika, B. C., & Milandou, C. (2019). Cartographie des forêts du Congo par télédétection dans le cadre du processus MRV-REDD+. *Revue Africaine des Sciences de l'Environnement, 4*, 67–82.

Pontius, R. G., Jr., Boersma, W., Castella, J.-C., Clarke, K., de Nijs, T., Dietzel, C., Duan, Z., Fotsing, E., Goldstein, N., Kok, K., Koomen, E., Lippitt, C. D., McConnell, W., Mohd Sood, A., Pijanowski, B., Pithadia, S., Sweeney, S., Trung, T. N., Veldkamp, A. T., & Verburg, P. H. (2008). Comparing the input, output, and validation maps for several models of land change. *The Annals of Regional Science*, 42(1), 11–37. https://doi.org/10.1007/s00168-007-0138-2

Pontius, R. G., & Millones, M. (2011). Death to Kappa: Birth of quantity disagreement and allocation disagreement for accuracy assessment. *International Journal of Remote Sensing, 32*(15), 4407–4429.

Potapov, P. V., Turubanova, S. A., Hansen, M. C., Adusei, B., Broich, M., Altstatt, A., Mane, L., & Justice, C. O. (2012). Quantifying forest cover loss in Democratic Republic of the Congo, 2000–2010, with Landsat ETM+ data. *Remote Sensing of Environment*, 122, 106–116. https://doi.org/10.1016/j.rse.2011.08.027

République du Congo. (2021). *Contribution déterminée au niveau national révisée (CDN 2021)*. Ministère de l'Environnement.

Riitters, K., Wickham, J., O'Neill, R., Jones, B., & Smith, E. (2000). Global-scale patterns of forest fragmentation. *Conservation Ecology, 4*(2), 3.

Rodriguez-Galiano, V. F., Ghimire, B., Rogan, J., Chica-Olmo, M., & Rigol-Sanchez, J. P. (2012). An assessment of the effectiveness of a random forest classifier for land-cover classification. *ISPRS Journal of Photogrammetry and Remote Sensing, 67*, 93–104.

Ruiz Pérez, M., Ezzine de Blas, D., Nasi, R., Sayer, J. A., Sassen, M., Angoue, C., Gami, N., Ndoye, O., Ngono, G., Nguinguiri, J. C., Nzala, D., Toirambe, B., & Yalibanda, Y. (2005). Logging in the Congo Basin: A multi-country characterization of timber companies. *Forest Ecology and Management, 214*(1–3), 221–236. https://doi.org/10.1016/j.foreco.2005.04.055

Sasaki, N., & Putz, F. E. (2009). Critical need for new definitions of "forest" and "forest degradation" in global climate change agreements. *Conservation Letters, 2*(5), 226–232.

Setiono, B. A., Fajri, M., Wibowo, A., & Hamzah, A. (2023). Assessment of land use/land cover change using Cellular Automata-Markov model: A systematic review. *Remote Sensing Applications: Society and Environment, 31*, 100997.

Shapiro, A. C., Aguilar-Amuchastegui, N., Hostert, P., & Bastin, J.-F. (2021). Forest degradation: Definitions, measures and field monitoring in African forests. *Ecological Indicators, 122*, 107310.

Shapiro, A., d'Annunzio, R., Desclée, B., Jungers, Q., Koy Kondjo, H., Mbulito Iyanga, J., Inicko Gangyo, F., Nana, T., Obame, C. V., Milandou, C., Rambaud, P., Sonwa, D. J., Mertens, B., Tchana, E., Khasa, D., Bourgoin, C., Ouissika, C. B., & Kipute, D. D. (2023). Small scale agriculture continues to drive deforestation and degradation in fragmented forests in the Congo Basin (2015–2020). *Land Use Policy, 134*, 106922. https://doi.org/10.1016/j.landusepol.2023.106922

Shapiro, A. C., Bernhard, K. P., d'Annunzio, R., Siwe, R., Iyanga, J. M., Obame, C. V., Mofack, G., II, Gangyo, F. I., Tchana, É., Arquero, A., Mbenza, D., Kondjo, H., Sannier, C., Mertens, B., Martins, F., & Vollrath, A. (2026). National forest cover change baselines for six countries of the Congo basin using

open-source solutions and sample-based area estimates (2015–2023). *Environmental Research Letters, 21*(9), 094028. https://doi.org/10.1088/1748-9326/ae61cd

Tadese, S., Soromessa, T., & Bekele, T. (2021). Analysis of the current and future prediction of land use/land cover change using remote sensing and the CA-Markov model in Majang Forest Biosphere Reserves of Gambella, Southwestern Ethiopia. *The Scientific World Journal, 2021*, 6685045.

Tchatchou, B., Sonwa, D. J., Ifo, S., & Tiani, A. M. (2015). *Deforestation and forest degradation in the Congo Basin: State of knowledge, current causes and perspectives* (CIFOR Occasional Paper). CIFOR. https://doi.org/10.17528/cifor/005894

Tiye, F. S., Korecha, D., Gutema, T. M., & Gemeda, D. O. (2025). Modeling land use and land cover dynamics of Bale Mountains National Park using Google Earth Engine and cellular automata–artificial neural network (CA-ANN) model. *PLOS ONE, 20*(4), e0320428. https://doi.org/10.1371/journal.pone.0320428

Tritsch, I., Le Velly, G., Mertens, B., Meyfroidt, P., Sannier, C., Makak, J.-S., & Houngbedji, K. (2020). Do forest-management plans and FSC certification help avoid deforestation in the Congo Basin? *Ecological Economics*, 175, 106660. https://doi.org/10.1016/j.ecolecon.2020.106660

Tyukavina, A., Hansen, M. C., Potapov, P., Parker, D., Okpa, C., Stehman, S. V., Kommareddy, I., & Turubanova, S. (2018). Congo Basin forest loss dominated by increasing smallholder clearing. *Science Advances*, 4(11), eaat2993. https://doi.org/10.1126/sciadv.aat2993

Umunay, P. M., Gregoire, T. G., Gopalakrishna, T., Ellis, P. W., & Putz, F. E. (2019). Selective logging emissions and potential emission reductions from reduced-impact logging in the Congo Basin. *Forest Ecology and Management, 437*, 360–371. https://doi.org/10.1016/j.foreco.2019.01.049

UNESCO. (1988). *Procès-verbal de la création de la Réserve de biosphère de Dimonika dans le cadre du Programme sur l'Homme et la Biosphère (MAB)*.

Wilson, M. C., Chen, X.-Y., Corlett, R. T., Didham, R. K., Ding, P., Holt, R. D., Holyoak, M., Hu, G., Hughes, A. C., Jiang, L., Laurance, W. F., Liu, J., Pimm, S. L., Robinson, S. K., Russo, S. E., Si, X., Wilcove, D. S., Wu, J., & Yu, M. (2016). Habitat fragmentation and biodiversity conservation: Key findings and future challenges. *Landscape Ecology*, 31(2), 219–227. https://doi.org/10.1007/s10980-015-0312-3

Woodcock, C. E., Allen, R., Anderson, M., Belward, A., Bindschadler, R., Cohen, W., Gao, F., Goward, S. N., Helder, D., Helmer, E., Nemani, R., Oreopoulos, L., Schott, J., Thenkabail, P. S., Vermote, E. F., Vogelmann, J., Wulder, M. A., & Wynne, R. (2008). Free access to Landsat imagery. *Science*, 320(5879), 1011. https://doi.org/10.1126/science.320.5879.1011a

Wulder, M. A., Loveland, T. R., Roy, D. P., Crawford, C. J., Masek, J. G., Woodcock, C. E., Allen, R. G., Anderson, M. C., Belward, A. S., Cohen, W. B., Dwyer, J., Erb, A., Gao, F., Griffiths, P., Helder, D., Hermosilla, T., Hipple, J. D., Hostert, P., Hughes, M. J., … Zhu, Z. (2019). Current status of Landsat program, science, and applications. *Remote Sensing of Environment*, 225, 127–147. https://doi.org/10.1016/j.rse.2019.02.015

Yuh, Y. G., N'Goran, K. P., Kross, A., Heurich, M., Matthews, H. D., & Turner, S. E. (2024). Monitoring forest cover and land use change in the Congo Basin under IPCC climate change scenarios. *PLOS ONE, 19*(12), e0311816. https://doi.org/10.1371/journal.pone.0311816

Zhu, Z., & Woodcock, C. E. (2012). Object-based cloud and cloud shadow detection in Landsat imagery. *Remote Sensing of Environment, 118*, 83–94.